Using a novel PV-Cre rat model to characterize pallidonigral cells and their terminations

DOCTORAL DISSERTATION

A thesis submitted in partial fulfillment
of the requirements for the degree of
Doctor of Philosophy

By:
Yoon-Mi Oh

Supervisor:
Dr. Fumino Fujiyama

Co-supervisor:
Dr. Fuyuki Karube
Dr. Susumu Takahashi

Graduate School of Brain Science
Doshisha University
March 2017
Kyoto, Japan

Abstract

In the present study, we generated a novel parvalbumin (PV)-Cre rat model and conducted a detailed morphological and electrophysiological investigation of axons from PV-globus pallidus (GP). The GP is considered a relay nucleus in the indirect pathway of the basal ganglia (BG). Previous studies have used molecular profiling and projection patterns to demonstrate cellular heterogeneity in the GP; for example, PV-expressing neurons are known to comprise approximately 50% of GP neurons and represent majority of prototypic neurons that project to the subthalamic nucleus and/or output nuclei of BG, entopeduncular nucleus and substantia nigra (SN). The present study aimed to identify the characteristic projection patterns of PV neurons in the GP (PV-GP neurons) and determine whether these neurons target dopaminergic or GABAergic neurons in SN pars compacta (SNc) or reticulata (SNr), respectively. We initially found that 1) 57% of PV neurons co-expressed Lim-homeobox 6, 2) the PV-GP terminals were preferentially distributed in the ventral part of dorsal tier of SNc, 3) PV-GP neurons formed basket-like appositions with the somata of tyrosine hydroxylase, PV, calretinin and cholecystokinin immunoreactive neurons in the SN, and 4) in vitro whole cell recording during optogenetic photo-stimulation of PV-GP terminals in SNc demonstrated that PV-GP neurons strongly inhibited dopamine neurons via $GABA_A$ receptors. These results suggest that dopamine neurons receive direct focal inputs from PV-GP prototypic neurons. The identification of high contrast inhibitory systems on dopamine neurons might represent a key step toward understanding the BG function.

Acknowledgement

First, I would like to express my sincere gratitude to my advisors, Prof. Fumino Fujiyama, Dr. Fuyuki Karube and Dr. Susumu Takahashi, for their continuous support of my Ph.D study inducing me to widen my research from various perspective. Their guidances helped me in all the time of research and writing of this thesis.

I would also like to thank to Prof. Kazuto Kobayashi and Kenta Kobayashi for providing PV-Cre rat and specified virus vector to succeed my research.

I could not have imagined having a better advisor and mentor for my Ph.D study.
Besides my advisor, I would like to thank the rest of my thesis committee: Prof. Yoshio Sakurai, Prof. Nobuyuki Nukina, and Dr. Junnya Hirokawa, for their encouragement, insightful comments, and meaningful questions.

I thank my fellow labmates in Neural circuitry Group: Kazuko Mizutani, Yasutake Nakano, Tetsuya Higasiyama, and Kumiko Ogata for their time, support, and helpful comments.

Last but not the least, I would like to thank my family: especially my parents for giving birth to me at the first place and supporting me spiritually throughout my life.

Table of contents

Chapter 1. General introduction ……. 9

1.1. Basis of basal ganglia network model …….. 9

1.2. Regulative innervation to dopaminergic neurons in SNc …… 12

1.3. Pallidonigral projection from GP ……12

1.4. Morphological Character and Molecular profile of GP …….. 13

Chapter 2. Materials & Methods…….16

2.1. Generation of transgenic rats ……...16

2.2. Tissue processing ……17

2.3. Animals and Surgery …….. 21

2.4. Analysis of PV-GP bouton distribution in the SN …… 22

2.4.1. Identification and subdivision of SNc area ……22

2.4.2. Estimation of the location of boutons and size of cell bodies in fluorescence images …….. 24

2.5. Slice preparation and whole-cell recording …… 25

2.5.1. Slice preparation …… 25

2.5.2. Immunohistochemistry for in vitro slice preparation …… 26

2.5.3. Analysis of electrophysiological data …… 27

Chapter 3. Results …… 29

3.1. Specificity of Cre expression in PV-Cre transgenic rats ……..… 29

3.2. Neuronal subpopulations of GP …… 33

3.3. Projection of axon fibers from PV neurons in the GP to the SN ……... 36

3.4. PV-GP neurons innervate the dopaminergic SNc and GABAergic SNr neurons …. 51

3.5. PV-GP neurons inhibit the dopaminergic SNc neurons …… 54

Chapter 4. Discussion ……... 59

4.1. Technical validation of the specificity of Cre expression in PV-Cre rats …….… 59

4.2. Molecular architecture of GP neurons ……... 60

4.3. Projection of pallidonigral neurons …… 61

4.3.1. Pallidonigral projections preferentially innervate the ventral tier of SNcd ….. 61

4.3.2. Pallidonigral projections formed basket-like somatic apposition ……. 62

4.3.3. PV-GP neurons inhibit to dopaminergic neurons in SNc ……. 63

4.3.4. Roll of pallidonigral projection in the BG network model ……64

Chapter 5. References …….. 66

Table of Figures

Figure 1. Schematic diagram of the basal ganglia network model ……... 11

Figure 2. Procedure for subdivision of the SN area ……..…….. 23

Figure 3. Distribution of Cre and parvalbumin (PV) immunoreactivity in the central nervous system (CNS) of PV-Cre transgenic rats …… 30

Figure 4. Double immunofluorescence labeling for Cre and parvalbumin (PV) immunofluorescence in the globus pallidus (GP) of PV-Cre rats …… 32

Figure 5. Immunohistochemical identification of the globus pallidus (GP) neuron classes …… 34

Figure 6. Spatial distribution and co-expression of PV and Lhx6 in the GP neurons. ……. 35

Figure 7. Efficient labeling of PV neurons using AAV vector encoding loxP in PV-Cre rats …… 37

Figure 8. tdTomato fluorescence, PV (blue) and Lhx6 (green) immunoreactivities in parvalbumin (PV)–Cre rats at 2 weeks after viral injection ……. 38

Figure 9. AAV vector used here did not label neurons retrogradely ……..... 39

Figure 10. Fluorescent images of axons in the substantia nigra pars compacta (SNc) and reticulata (SNr) originated from parvalbumin (PV)–globus pallidus (GP) neurons……... 41

Figure 11. Fluorescent images of axons from parvalbumin (PV)–globus pallidus (GP) neurons in the substantia nigra pars compacta (SNc) and reticulata (SNr) …….. 42

Figure 12. Spatial distribution of PV-GP axon boutons near the border between substantia nigra pars compacta (SNc) and pars reticulata (SNr) …….. 45

Figure 13. Fluorescent images of CB, CCK, CR or NOS-positive cell body and axons from PV-GP neurons in the SN ……...…….…….……... 47

Figure 14. Estimated distances between the centers of the TH-positive cell bodies and PV-GP boutons ……..…….……. 48

Figure 15. Estimated distances between the centers of the PV-positive cell bodies and PV-GP boutons ……..…….……. 49

Figure 16. Estimated distances between the centers of the CB, CCK, CR or NOS-positive cell bodies and PV-GP boutons ..…….…….. 50

Figure 17. PV-GP neurons formed large and dense axon varicosities in the ventral part of the SNcd and SNr ……... 52

Figure 18. Somatic apposition on substantia nigra (SN) neurons by parvalbumin (PV)-globus pallidus (GP) axon terminals associated with the GABAergic post-synaptic marker, gephyrin ……. 53

Figure 19. Globus pallidus (GP) axon terminals of parvalbumin (PV) neurons elicited inhibitory postsynaptic currents (IPSCs) in dopaminergic neurons of substantia nigra pars compacta (SNc) …….……..... 56

Abbreviation list

BG; Basal ganglia

EP; Entopeduncular nucleus

GP; Globus pallidus

STN; Subthalamic nucleus

SN; Substantia nigra

SNc; Substantia nigra pars compacta

SNcd; Dorsal tier of substantia nigra pars compacta

SNcv; Ventral tier of substantia nigra pars compacta

SNr; Substantia nigra pars reticulata

VP; Ventral pallidum

Lhx6; Lim-homeobox 6

PV; Parvalbumin

CR; Calretinin

CCK; cholecystokinin

CB; calbindin

NOS; Nitric oxide synthase

AAV; Adeno-associated virus vector

TH; Tyrosine hydroxylase

FoxP2; Forkhead box protein P2

NKx2-1; NK2 homeobox 1

GABA; Gamma-Aimnobutyric acid

LM; Lateromedial

Chapter 1. General Introduction

1.1. Basis of basal ganglia network model

The basal ganglia (BG) is involved in motor control through the two main pathways with the opposite function : the direct pathway and the indirect pathway, and their circuitry and functions have been revealed by tons of morphological and electrophysiological researches in primates and rodents (DeLong et al. 1985; Robledo and Ferger 1990; Kincaid et al. 1991; Kita and Kitai 1991; Wichmann et al. 1994; Jaeger et al. 1995; Parent and Hazrati 1995a; Parent and Hazrati 1995b; Bergman et al. 1998; Mounir and Parent 2002). The dichotomy between direct and indirect pathways start at the striatum, which receives excitatory inputs from the cortex and the thalamus, thus is considerd as the input nucleus of the BG pathway model (Figure 1). Two projection neuron types in the striatum are clearly segrerated on both molecular expressions and projections. One type is the direct pathway medium spiny neurons (dMSNs),which express gamma-aminobutyric acid (GABA), dynorphin, substance P, and D1 receptor, and send the inhibitory projection to the output nuclei of the BG, the entopeduncular nucleus (EP; homologous to the internal segment of globus pallidus in primates) and the substantia nigra (SN). Those output nuclei autonomously inhibit thalamus and other brain areas, which are responsible for facilitating the voluntary movement, thus SN and EP suppress motor behaviors. Once dMSNs are activated by cortical and/or thalamic excitatory inputs, they inhibit activities of SN and EP. In turn, thalamus and other brain areas innervated by SN and EP are released from inhibition,

namely,disinhibition occurs. As a result, motor behaviors are facilitated. In contrast, another projection neuron type of the striatum, indirect pathway medium spiny neurons (iMSNs), which express GABA, encephalin and D2 receptor, do not project to the BG output nuclei directly. Rather, they project to the globus pallidus (GP), which is homologous to the external GP segment in primates. Then, GP and subthalamic nucleus (STN) innervate the output nuclei. Indirect pathway has one extra step compared to direct pathway. Therefore, activating iMSNs inhibit GP, then SN and EP are released from autonomous inhibition by GP, and they inhibit thalamus and other brain area. As a result voluntary movement suppresses. Taken together, direct pathway functions as an 'accelerator pedal' and indirect pathway as a "brake pedal" of voluntary movement, respectively, that operates regulatory related to activate movements (Haber and Watson 1985; Haber et al. 1993; Kita and Kitai 1994; Bevan et al. 1998; Smith et al. 1998; Bevan et al. 2002; Kita 2007; Stephenson-Jones et al. 2011). In this model of the BG, GP is thought to be primarily function as a relay nucleus in the indirect pathway. Projections from dopamiergic neurons of the SNc widely innervate the striatum. By dopaminergic inputs, direct pathway neurons in the striatum are activated their function through D1 receptors while indirect neurons are modified to suppress function through D2 receptor.

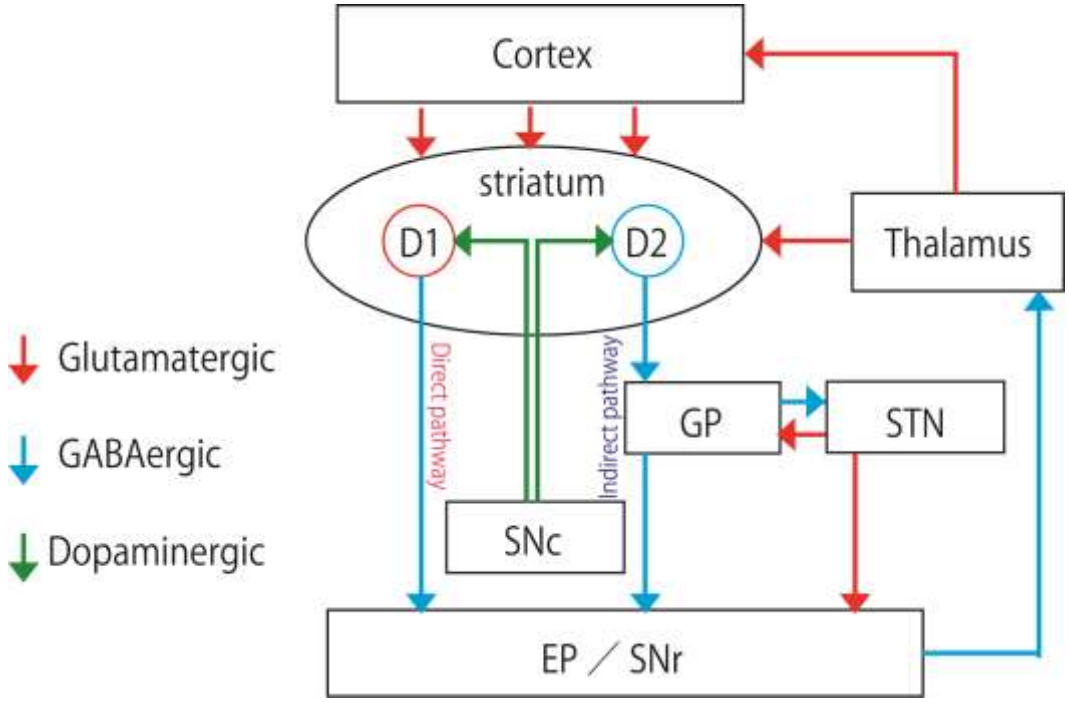

Fig. 1 Schematic diagram of the basal ganglia network model

Excitatory projections are shown as red arrows, and inhibitory projections as blue arrows. In this model, the striatum, which is the input nucleus, receives the excitatory inputs from the cortex and the thalamus. Subsequently, striatal information is sent to the output nuclei, the entopeduncular nucleus (EP) and the substantia nigra pars reticulata (SNr), in direct pathway. On the other hamd, striatal information is provided output nuclei via globus pallidus (GP) and subthalamic nucleus (STN) in the indirect pathway. Furthermore, functions of both two pathways are modified by dopaminergic inputs from substantia nigra pars compacta (SNc), shown as green arrows.

1.2. Regulatiive innervation to dopaminergic neurons in SNc

Dopaminergic neurons are located primarily in the SN pars compacta (SNc), where they are further classified as neurons of the SNc dorsal tier (SNcd) and ventral tier (SNcv). GABAergic neurons are located in the SN pars reticulata (SNr), which projects to the thalamus, superior colliculus, and pedunculopontine tegmental nucleus (Gerfen et al. 1982). SNc dopaminergic neurons have a strong influence on emotion, motivation, cognitive processes and motor control, it is important to know how they are innervated. Around 70% of inputs to SNc are GABAergic (Bolam and Smith 1990), arising from the striatum (Bolam and Smith 1990; Paladini et al. 1999), SNr (Paladini et al. 1999) and VP (Groenewegen et al. 1993). Previously, It has been reported that SNc dopaminergic neurons receive the GABAergic projections from direct pathway neurons only in striosome compartment of the striatum, which also project to the EP and the SNr of the output nuclei (Gerfen et al., 1985; Kawaguchi et al., 1990; Fujiyama et al., 2011; Watabe-Uchida et al., 2012). In addition, GP, which is known as relay nucleus in indirect pathway, also provides inhibition onto SNc neurons (Smith and Bolam 1989; Tepper et al. 1995; Paladini et al. 1999; For review, see Tepper and Lee 2007). However, it is unclear what cell types of GP neurons input to SNc, and effect of pallidonigral input on SNc dopaminergic neurons.

1.3. Pallidonigral projection from GP

Currently, the proportions of pallidonigral fibers that terminate in the SNc versus the SNr remain unclear. For example, some researchers have described pallidonigral projection as a system of

fibers that arborize to a similar extent in both the SNc and SNr (Kim et al. 1976; Carter and Fibiger 1978; Nauta 1979; DeVito and Anderson 1982). In contrast, others consider the SNr, rather than the SNc, to be the major site of pallidonigral fiber termination (McBride and Larsen 1980; Haber and Watson 1985; Smith and Bolam 1990a). Anterograde tracing study with the injection of Phaseolus vulgaris leucoagglutinin demonstrated that neurons in the lateral part of the GP innervated the central core of the rostral three quarters of the SNr, but only few fibers from the most medial part of the GP targeted SNr (Smith and Bolam 1989). Conventional anterograde tracers can also label passing fibers, thus, the results need to be interpreted carefully. The one of reliable methods is to use transgenic animals in which a specific type of neurons expresses Cre and/or fluorescent proteins. Genetic strategy in mice combining the Cre/loxP gene expression system and rabies-virus-based transsynaptic retrograde tracing revealed that the GP projected to SNc dopamine rgicneurons in mice (Watabe-Uchida et al. 2012), although the molecular characteristics of the GP neurons remained unknown. Only an exception was the report which observed that GP axons in the SNc arose mostly from Lim-homeobox 6 (Lhx6)-expressing neurons and parvalbumin (PV)-GP neurons targeted mainly SNr (Mastro et al. 2014).

1.4. Morphological Character and Molecular profile of GP neurons

Several reports provided evidences for cellular heterogeneity of the GP (Kita and Kitai 1994; Nambu and Llinas 1994; Nambu and Llinás 1997; Hoover and Marshall 2002; Kita 2007; Sadek et al. 2007; Flandin et al. 2010; Gittis et al. 2014; Abdi et al. 2015; Dodson et al. 2015). A recent

study of transgenic mice also found that Lhx6- and PV-expressing neurons comprised genetically distinct cell populations that each accounted for a third of neurons in the GP. However, estimates of the numbers of PV-GP neurons and their coexistence with other neurons, especially those expressing Lhx6, differ vastly among research groups and species of animals (Flandin et al. 2010; Nóbrega-Pereira et al. 2010; Abdi et al. 2015; Dodson et al. 2015; Hernandez et al. 2015). In rats, Mallet et al. defined two populations of GP neurons by electrophysiological features, molecular profiles and axonal connectivity in Parkinsonian rats (Mallet et al. 2012). The first population of prototypic GABAergic GP neurons fire antiphase to subthalamic STN neurons, often express PV, and target downstream basal ganglia nuclei, including STN. In contrast, the second population (arkypallidal neurons) expressing fire in–phase with STN neurons preproenkephalin, and innervate only the striatum (Mallet et al. 2012). In healthy rats, Abdi et al. showed that two-thirds of all GP neurons were identified by co-expression of Nkx2-1 and Lhx6 (with many also expressing PV and ER81) and further revealed that Lhx6^{+}/PV^{+} neurons, the major population of GP, were prototypic neurons (Abdi et al. 2015). These reports were based on excellent immunohistochemistry to identify GP neuron types, however, it will be highly more useful if specific population of GP neurons was genetically labelled in rats. The SN, one of the projection targets of GP neurons, comprises two main types of neurons, classified according to the use of dopamine or GABA as a neurotransmitter.

However, as the above written, identification of GP neuron types is bit contradictory, therefore it

remains unclear innervation pattern of PV-expressing neurons onto SNc dopaminergic neurons. Given the functional importance of the basal ganglia in motor control and reward based learning, the question of whether PV-GP neurons target SNc dopaminergic or SNr GABAergic neurons is important. To address this question, we first generated a transgenic rat model to express Cre transgene under the control of the PV gene promoter and subsequently investigated the innervation of SN neurons by PV-GP neurons using morphologic and electrophysiological methods.

Chapter 2. Materials and Methods

All animal experiments were approved and performed in accordance with the guidelines for the care and use of laboratory animals established by the Animal Experiments Committee of Fukushima Medical University and by the Committee for Animal Care and Use and Committee for Recombinant DNA Study of Doshisha University. All efforts were made to minimize animal suffering and the number of animals used. For anatomical experiments, 3 wild type and 14 PV-Cre Long Evans background transgenic rats were used (postnatal 8-9 week-old). Other 7 PV-Cre rats were used for electrophysiological experiments (postnatal 29-41 day-old). Chemicals were derived from Nacalai Tesque (Kyoto, Japan) and Wako (Osaka, Japan), unless otherwise noted.

2. 1. Generation of transgenic rats

The transgene construct contained the Cre recombinase coding sequence with a nuclear localization signal in the place of the initiation codon of the mouse PV gene on a bacterial artificial chromosome clone (Tanahira et al. 2009). This construct was linearized by PI-SceI digestion and purified by pulse field gel electrophoresis and microinjected into fertilized Long Evans rat eggs, which were implanted into pseudopregnant females. Transgenic rats were identified by Southern blot hybridization or PCR with genomic DNA prepared from tail clips. From fifteen transgenic rat founders generated, one transgenic line (termed PV-Cre/2-28) was selected as it expressed Cre gene

in PV-positive neurons most frequently based on the histological data obtained from double immunostaining for Cre and PV (for details, see Results).

2. 2. Tissue processing

Male and female rats were deeply anesthetized with isoflurane (Pfizer Japan Inc., Tokyo, Japan) and then with overdose of sodium pentobarbital (100 mg/kg, intraperitoneal [i.p.]; Kyoritsu Seiyaku Corporation, Tokyo, Japan) and transcardially perfused with 0.05 M phosphate-buffered saline, pH 7.4 (PBS), followed by 4% formaldehyde and 75%-saturated picric acid in 0.1 M Na_2HPO_4 9 (adjusted using NaOH to pH 7.0). Adult rat brains were stored in fixative at room temperature for 4 h, followed by cryoprotection with 30% sucrose in PBS for 2 days at 4ºC. Tissue blocks containing the GP were sectioned sagittally using a freezing microtome (Leica Instruments, Wetzlar, Germany) at a thickness of 20 or 25 μm. Six series of floating sections were collected in 0.1 M PB containing 0.02% sodium azide and prepared for immunofluorescent staining of the GP molecular markers listed in Table 1 (Mallet et al. 2012; Abdi et al. 2015). After washing in PBS containing 0.3% Triton-X-100 (PBS-X), sections were incubated overnight at 4ºC with primary antibodies (Table 1) diluted in incubation buffer containing 10% (v/v) normal donkey serum, 2% bovine serum albumin, and 0.5% (v/v) Triton X-100 in PBS or 0.12% lambda-carrageenan, 0.02% sodium azide, and 1% donkey serum in 0.3% (v/v) PBS-X. After exposure to primary antibodies, sections were washed in PBS and incubated overnight at room temperature in the same buffer containing a mixture of fluorophore-conjugated secondary antibodies (Table 2). After another washing protocol,

sections were mounted on non-coated glass slides, air dried, and coverslipped with 50% (v/v) glycerol/TBS with or without Prolong Gold (anti-fading reagent; Thermo Fisher Scientific, Waltham, MA, USA) or Fluoro-KEEPER (Nacalai). Immunofluorescence was observed under an epifluorescent microscope (BX-61, Olympus, Tokyo, Japan) or a confocal microscope (FV1200, Olympus) with appropriate filter sets (359–371 nm excitation and ≥397 nm emission for Alexa Fluor (AF) 350 or 405; 450–490 nm excitation and 514–565 nm emission for AF488; 530–585-nm excitation and ≥615 nm emission for AF594 or tdTomato). Images of each channel were taken sequentially and separately to negate possible signal crosstalk across channels.

Table 1. Primary antibodies used for research purposes

Antigen	Host Species	Dilution	Supplier	Catalog no.
Cre	Mouse	1:250	EMD Millipore (Temecula, CA)	MAB3120
Gephyrin	Mouse	1:500	Synaptic Systems (Goettingen, Germany)	147011
FoxP2	Rabbit	1:2000	Abcam (Cambridge, UK)	ab16046
Lhx6	Mouse	1:1000	Santacruz (Dallas, Tex)	sc-271433
NeuN	Mouse	1:2000	Millipore	MAB377
NeuN	Rabbit	1:500	Millipore	ABN78
Parvalbumin	Guinea pig	1:2000	Synaptic Systems	195004
Tyrosine Hydroxylase	Mouse	1:2000	Millipore	MAB318
Tyrosine Hydroxylase	Rabbit	1:500	Millipore	AB152
NOS	Rabbit	1:5000	Sigma Aldrich (St. Louis, MO)	N7280
Calbindin	Rabbit	1:5000	Frontier Institute (Ishikari, Japan)	Calbindin-Rb-Se-1
Calretinin	Rabbit	1:2000	Swant Swiss antibodies (Marly, Switzerland)	7697
CCK	Rabbit	1:5000	Sigma Aldrich	C2518

Table 2. Secondary antibodies and a fluorescent reagent used in research

Secondary Antibody and a fluorescent reagent	Host Species	Dilution	Supplier	Catalog no.
Anti-mouse Alexa Fluor®350	Donkey	1:500	Thermo Fisher Scientific, Inc. (Waltham, MA)	A10035
Anti-mouse Alexa Fluor®405	Goat	1:500	Thermo Fisher Scientific, Inc.	A31553
Anti-mouse Alexa Fluor®488	Donkey	1:500	Thermo Fisher Scientific, Inc.	A21202
Anti-mouse Alexa Fluor®594	Goat	1:500	Thermo Fisher Scientific, Inc.	A11032
Anti-mouse Alexa Fluor®635	Goat	1:500	Thermo Fisher Scientific, Inc.	A31575
Anti-guinea pig Alexa Fluor®488	Goat	1:500	Thermo Fisher Scientific, Inc.	A11073
Anti-guinea pig Alexa Fluor®594	Goat	1:500	Thermo Fisher Scientific, Inc.	A11076
Anti-guinea pig Alexa Fluor®633	Goat	1:500	Thermo Fisher Scientific, Inc.	A21105
Anti-rabbit Alexa Fluor®350	Donkey	1:500	Thermo Fisher Scientific, Inc.	A10039
Anti-rabbit Alexa Fluor®488	Goat	1:500	Thermo Fisher Scientific, Inc.	A11034
Anti-rabbit Alexa Fluor®546	Donkey	1:500	Thermo Fisher Scientific, Inc.	A10040
Anti-rabbit Alexa Fluor®635	Donkey	1:500	Thermo Fisher Scientific, Inc.	A31577
CF350-streptavidin		1:2000	Biotium (Fremont, CA)	29031

2. 3. Animals and Surgery

Male and female rats were anesthetized by inhalation of isoflurane followed by intramuscular injection of mixture of ketamine (Ketalar; Daiichi-Sankyo, Tokyo, Japan; 40 mg/kg) and xylazine (Bayer HealthCare, Tokyo, Japan; 4 mg/kg). Each rat was then fixed to a stereotaxic device (Narishige, Tokyo, Japan), and the skull was drilled to make a small hole in an appropriate position in accordance with the rat brain atlas (Paxinos and Watson 2007). For GP neuron axon labeling, 0.1 to 0.2 μL of a viral vector (1.5×10^{10} vg/μL AAV-FLEX-rev-ChR2- tdTomato; a gift from Scott Sternson; Addgene plasmid # 18917; for details see Atasoy et al., 2008) was injected into the GP [anteroposterior (AP): 1.4 to 1.6 mm caudal from the bregma, lateromedial (LM): 3.2 to 3.4 mm lateral from the midline, depth: 6.2 mm from the pial surface] using a glass pipette (tip diameter, 20–30 μm) through which air pressure pulses were delivered with a pressure injector (PV820, World Precision Instruments, Sarasota, FL, USA). Each rat was perfused least 2 weeks after AAV injection, and tissues were prepared as described above.

2. 4. Analysis of PV–GP bouton distribution in the SN

Triple-fluorescent 2-dimensional (2D)-images of the SN were captured as 8-bit RGB images at LM 1.9 mm, which contained the most intense PV–GP axon terminals. In these images, the fluorescence of the axons infected with AAV and immunoreactivity of TH and PV were detected in the red, blue, and green channels, respectively. For each image, each channel was analyzed separately as described below.

2. 4. 1. Identification and subdivision of SNc area

The area of SNc was defined by TH immunoreactivity and a contour of SNcd was plotted by Neurolucida (MBF Bioscience, Inc., Williston, VT, USA), which was consisted of two polygonal lines, top and bottom ones (white and red lines in Fig. 12C in Page 45, respectively). The top one was the dorsal edge of SNcd and the bottom was the border between SNc and SNr. To quantify bouton distribution around the border region between SNc and SNr, we divided the area into four sub-areas as shown in Fig. 2. Firstly, the leftmost and rightmost positions of the polygon surrounding SNcd were identified, respectively to determine the horizontal axis. The horizontal axis was equally divided into 100 sections, from which perpendicular lines were drawn to cross with the top and bottom SNc polygons. Points that bisect each perpendicular line intersecting the polygons were identified. A polygonal line that connects all the bisection points was defined as a border area I and area II, which divide the SNcd into 2 sub-areas, dorsal and ventral ones. Points that are arranged symmetrically against the bisection point in the vertical direction with the border between SNc and SNr as the axis of symmetry at each divided location were identified, and then a polygonal line that connect the points was defined as a border between area III and area IV, which contains the most dorsal part of SNr. Similarly, points that are arranged symmetrically against the point on the border between SNc and SNr in the vertical direction with the border between area III and area IV as the axis of symmetry at each divided location were identified, and then a polygonal line that connect the points was defined as a bottom edge of all the areas. Within the area, axonal

boutons of PV-GP neurons were manually plotted using Neurolucida and the number of boutons located in the sub-area I, II, III and IV was counted. Statistical comparison among the sub-area was examined by Friedman test with Bonferroni's post-hoc multiple-comparison.

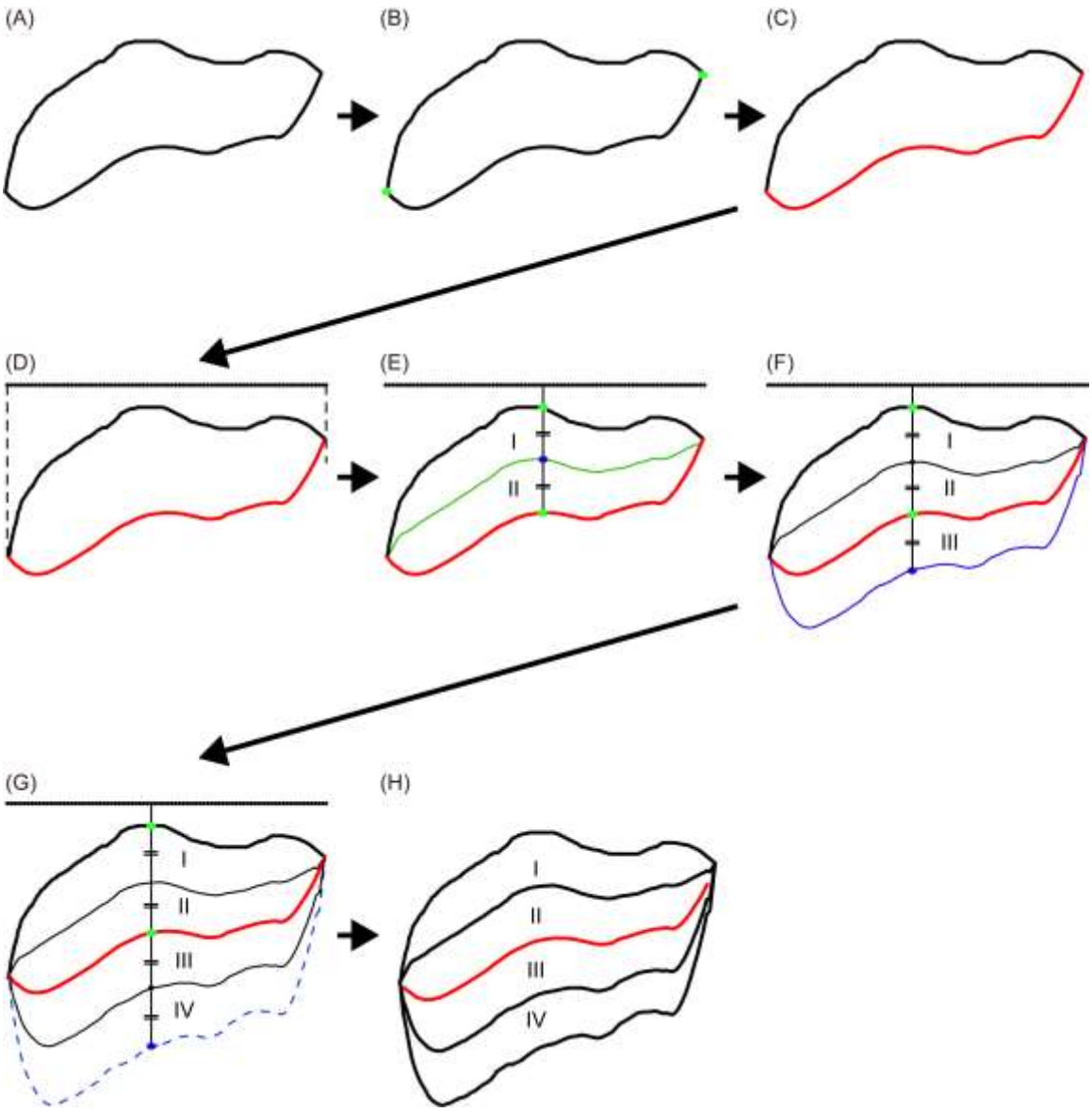

Fig. 2 Procedure for subdivision of the SN area

(A) The area of SNc was defined by TH immunoreactivity. (B) The leftmost and rightmost positions of the polygon were identified, respectively (green dots). (C) The bottom polygonal line (red) was defined as the border between SNc and SNr. (D) A line connecting coordinates of the horizontal axis of the positions was equally divided into 100 positions (top dots). (E) At each divided position, points that bisect a perpendicular line intersecting the polygon were identified (ex. blue dot). A polygonal line that connects all the bisection points was defined as a border between area I and area II (green polygonal line). (F) Points that are arranged symmetrically against the

bisection point in the vertical direction with the border between SNc and SNr as the axis of symmetry at each divided location were identified, and then a polygonal line that connects the points was defined as a border between area III and area IV (blue polygonal line). (G) Points that are arranged symmetrically against the point on the border between SNc and SNr in the vertical direction with the border between area III and area IV as the axis of symmetry at each divided location were identified, and then a polygonal line that connects the points was defined as a bottom edge of all the area (blue dotted polygonal line). (H) The identified four areas (I – IV) of SN.

2. 4. 2. Estimation of the location of boutons and location and size of cell bodies in fluorescence images

The immunohistochemically visualized cell bodies of TH-, PV-, calretinin (CR)-, cholecystokinin (CCK)-, calbindin (CB)- or nitric oxide synthase (NOS)-immunoreactive cells (Fig. 13 in Page 47) were also manually plotted by Neurolucida. To estimate the locations and sizes of the cells, the 'regionprops' function of Matlab (MathWorks, Inc., Natick, MA, USA) was used to identify circle-like structures in the plots as cells. The location and size of each identified cell were estimated by calculating the centroid and minimum axis length, respectively. Estimation of distance between a cell body center and the boutons Euclidian distances between an estimated cell centroid and all boutons were calculated on the basis of the estimated locations and sizes of cell, and the identified locations of bouton. Because fluorescence images were captured in a 2D plane that comprises a single slice of the three dimensional (3D) cell structure, the cell size on an image largely depended on the plane of the cut. Therefore, we normalized the Euclidian distance using half of the estimated size, defined as the distance from the cell center to the edge. Note that the estimated circle-like structures were defined as cells. Using this normalization, we examined the spatial distributions of boutons along 3D cell body surfaces in the 2D plane.

2. 5. Slice preparation and whole-cell recording

2. 5. 1. Slice preparation

AAV was injected as described above; only difference from above procedures was the age of the rats. At least 2 weeks after AAV injection, the rat was deeply anesthetized with sodium pentobarbital (100 mg/kg, i.p.) and intracardially perfused with ice-cold modified artificial cerebrospinal fluid (ACSF: NaCl 75; KCl, 2.5; $CaCl_2$, 0.7; $MgCl_2$, 2.0; $NaHCO_3$, 26; Glucose, 100; $NaHPO_4$, 1.25; pyruvic acid, 2; lactic acid, 4; all values in mM). All ACSF had been aerated with 95%/5% O_2/CO_2. Then, the brain was taken out and quickly incubated in modified ACSF for 2 min. Three hundred micrometer-thick sagittal slices were cut and incubated in modified ACSF at 32°C for 20 min and transferred to an incubation chamber at room temperature for at least 1 h. The recording chamber was perfused with standard ACSF (NaCl 125; KCl, 2.5; $CaCl_2$, 2.4; $MgCl_2$, 1.2; $NaHCO_3$, 25; Glucose, 15; $NaHPO_4$, 1.25; in mM) maintained at 30°C. To amplify inhibitory postsynaptic currents (IPSCs) as an inward current, a whole-cell glass pipette (4–7 MΩ) was filled with an intracellular solution with an elevated chloride concentration (KCl 135; NaCl 3.6; ATP 2; GTP 0.4; $MgCl_2$ 1; Na_4EGTA 0.5; HEPES 10; bicocytin 20.1; in mM) with a pH of 7.3 (adjusted by KOH) and osmolality of ~290 mOsm. The brain slice was observed by an epifluorescence microscope under IR-DIC configuration. The nucleus of SN was identified and the SNc was distinguished from the SNr by higher cell density. Almost no retrograde labeling was observed in the SN. Although our main targets were SNc neurons (N = 11), three SNr neurons were also recorded to just compare electrophysiological properties with those of SNc neurons, but were not

examined for optogenetic stimulation. Current or voltage clamp recordings were obtained by an EPC10 (HEKA Elektronik Dr. Schulze GmbH, Lambrecht/Pfalz, Germany) with a sampling rate of 20 kHz. Once cells were recorded in a whole-cell voltage clamp configuration, a voltage pulse (−5 mV for 10 ms) was applied repeatedly to monitor series resistance (<20 MΩ in our samples). Shortly (less than 1 min) after completing the whole-cell configuration, firing responses against 1 s depolarizing current pulses (maximum intensity, 1000 pA with a 50 pA step) were recorded. Then passive membrane properties were monitored by steps of hyperpolarized current pulses (1 s). For photo activation of ChR2, a 470 nm light-emitting diode (LED; Mightex Systems, Pleasanton, CA, USA) was used at full field illumination through a 40x water immersion objective. One to 10-ms blue light pulses were applied at a maximum total power of ~2 mW. In some experiments, low concentration of tetrodotoxin (1 μM) and 4-amino pyridine (100 μM) were added to ACSF to isolate monosynaptic currents (Shu et al. 2007; Petreanu et al. 2009). CNQX (10 μM) and AP5 (50 μM) were applied to inactivate glutamatergic synaptic currents (N = 3), and SR95531 (20 μM) was applied (N = 4) to examine the $GABA_A$ receptor dependency of IPSCs. All pharmacological reagents were purchased from Tocris Bioscience (Bristol, UK).

2. 5. 2. Immunohistochemistry for in vitro slice preparation

After recording session, the slice was fixed overnight in 4% paraformaldehyde and 0.2% picric acid in PB. The fixed slice was washed with PB and then embedded in agar and re-sectioned at a thickness of 50-μm by a vibratome. Biocytin-filled recorded neurons were visualized with

AF-conjugated streptavidin (1:1000–2000 dilution; Life Technologies, Carlsbad, CA, USA). To confirm whether recorded cells were dopaminergic neurons, sections were incubated overnight with primary antibodies against TH and PV (Table 1) in incubation buffer containing 10% normal donkey serum, 2% bovine blood serum albumin, and 0.5% Triton X in 0.05M PBS. After incubation sections were washed with PBS thrice, each for 10 min and incubated with the appropriate AF-conjugated (Table 2) or CF dye-labeled secondary antibodies (Table 2) for 3 h. Sections were rinsed, dried on a slide glass, and coverslipped with 50% (v/v) glycerol/TBS with Prolong Gold (anti-fading reagent; Thermo Fisher Scientific, Waltham, MA, USA). All sections were observed using an epifluorescent or confocal microscope.

2. 5. 3. Analysis of electrophysiological data

Electrophysiological data was analyzed using IgorPro (Wave Metrics Inc., Portland, OR, USA) with the Neuromatic plugin (http://www.neuromatic.thinkrandom.com). The input resistance was determined via the linear fitting of voltage responses to hyperpolarized current pulses (-20 to -100 pA with 20 pA steps). The membrane time constant was calculated from the response to a -50 pA current pulse. To identify IPSC, each trace was smoothed with a 0.2 ms moving time window (moving average of 4 consecutive recording points), and all traces were aligned with the onset of photostimulation to calculate the average trace. The peak amplitude was measured for the inward current with a stable delay after photostimulation. The inward current was identified as a photo-induced IPSC if the peak amplitude was 3-fold larger than the standard deviation (SD) of the

baseline. The baseline was defined as the mean current trace of the postsynaptic cell over a 50 ms period prior to corresponding photo stimulation. The IPSC amplitude was measured from the baseline to the peak of the IPSC. The rising phase of the IPSC was fitted linearly and extrapolated and the intersection point with the baseline was determined. The time of this intersection point was defined as the onset of the IPSC. Latency was measured as the time from the photo stimulation onset to that of the IPSC. The statistical analysis was conducted using IgorPro and R (http://www.r-project.org/; R Project for Statistical Computing, Vienna, Austria). Data are described as means ± standard deviations (SD), unless otherwise noted. The Wilcoxon signed-rank test was used to evaluate the statistical significance of paired data.

Chapter 3. Results

3. 1. Specificity of Cre expression in PV-Cre transgenic rats

To verify the specificity of Cre expression, we surveyed several brain regions with known PV expression (Fig. 3). The distribution of Cre-positive neurons in the brains of PV-Cre transgenic rats was carefully examined using double immunohistochemistry for Cre visualized with AF594 and compared with the PV immunoreactivity (AF488) (Fig. 3). High-magnification images showed a high degree of colocalization between Cre and PV in all examined regions (Fig. 3). Cre/PV neurons were scattered throughout the striatum (Fig. 3. A). In the output nuclei of the BG, Cre/PV neurons were largely confined to the center of EP (Fig. 3. B) and mainly distributed in SNr rather than SNc (Fig. 3. C). In other areas, Cre/PV neurons were distributed in layers 2 to 6 in the cerebral cortex (Fig. 3. D) and in the pyramidal cell layer of hippocampus CA1 and CA3, and occupied the full extent of the thalamic reticular nucleus (Rt) (Fig. 3. E, F). These expression profiles are consistent with previous reports of PV expression in rodent brains (DeFelipe 1993; Hontanilla et al. 1997; Klausberger and Somogyi 2008; Paxinos et al. 2009; Miyamoto and Fukuda 2015; Wheeler et al. 2015). These results indicate that Cre expression is specific to PV-expressing neurons in this rat line.

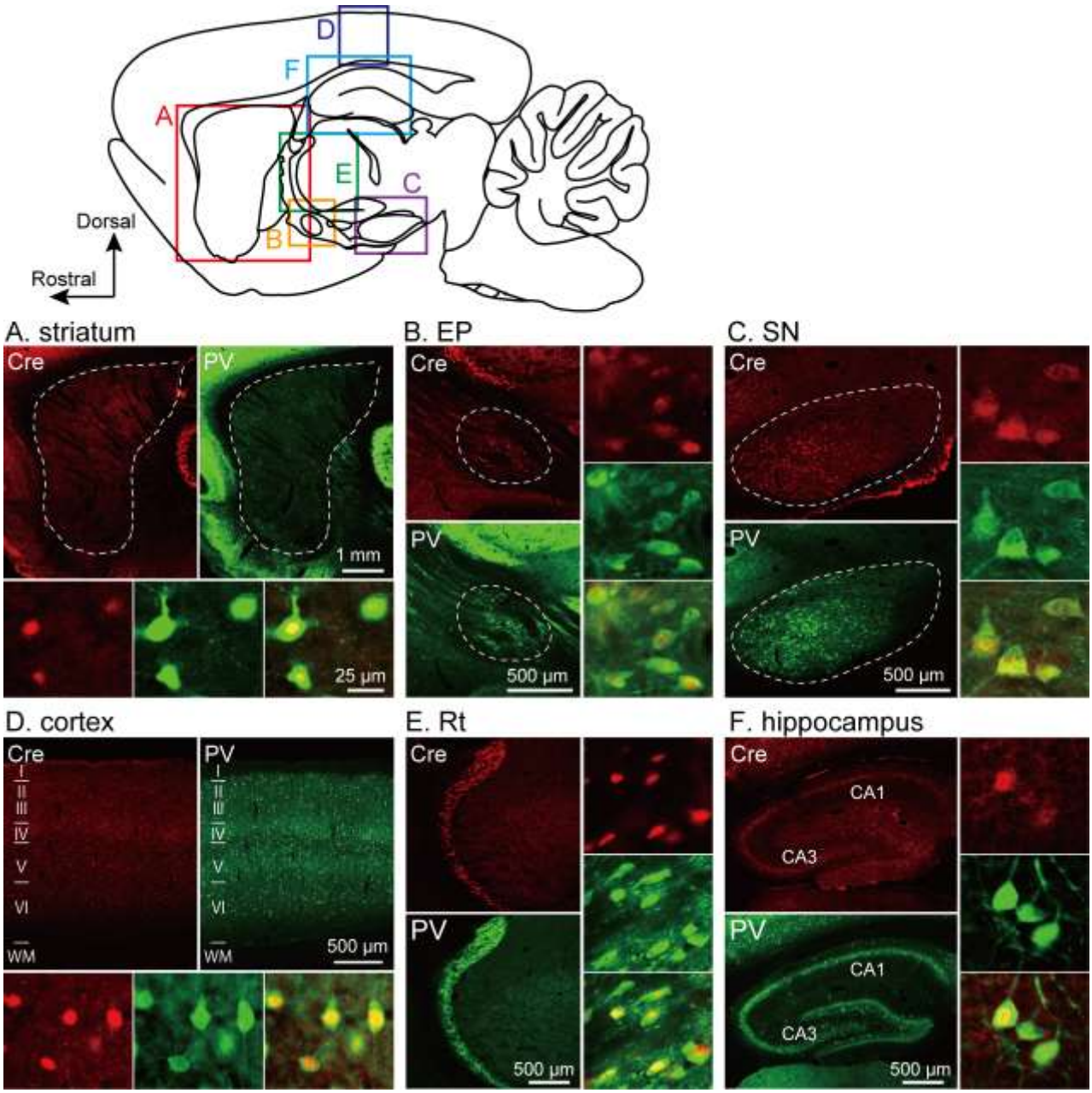

Fig. 3 Distribution of Cre and parvalbumin (PV) immunoreactivity in the central nervous system (CNS) of PV-Cre transgenic rats

Low- and high-magnification fluoroimages of Cre (AF594) and PV (AF488) immunoreactivity in the CNS were taken from the striatum (A), entopeduncular nucleus (EP, B), substantia nigra (SN, C), cortex (D), thalamic reticular nucleus (Rt, E), and hippocampus (F), as shown in the schematic. Photos were taken with an epifluorescent microscope (BX-61, Olympus, Tokyo, Japan) under the conditions described in the Materials and Methods.

Next, we quantitatively assessed PV expression in Cre- immunoreactive cells and vice versa in the GP by double immunofluorescence labeling for Cre (AF594) and PV (AF488) (Fig. 4A). The vast majority of Cre-immunoreactive neuronal cell bodies exhibited PV immunofluorescence (86.05 ± 6.13%, N = 1,943 cells from 9 sections in 3 rats, Fig. 4B, white columns). Likewise, the vast majority of PV- immunoreactive neuronal cell bodies (80.23 ± .84%, N = 2,063 cells from nine sections in three rats) exhibited Cre immunofluorescence (Fig. 4B, gray columns). We observed those results in 3 sagittal sections (lateromedial (LM) 3.9-4.0, 3.4, and 2.9 mm) in each rat, and a high degree of co-localization was observed almost consistently in the lateral-medial axis of GP.

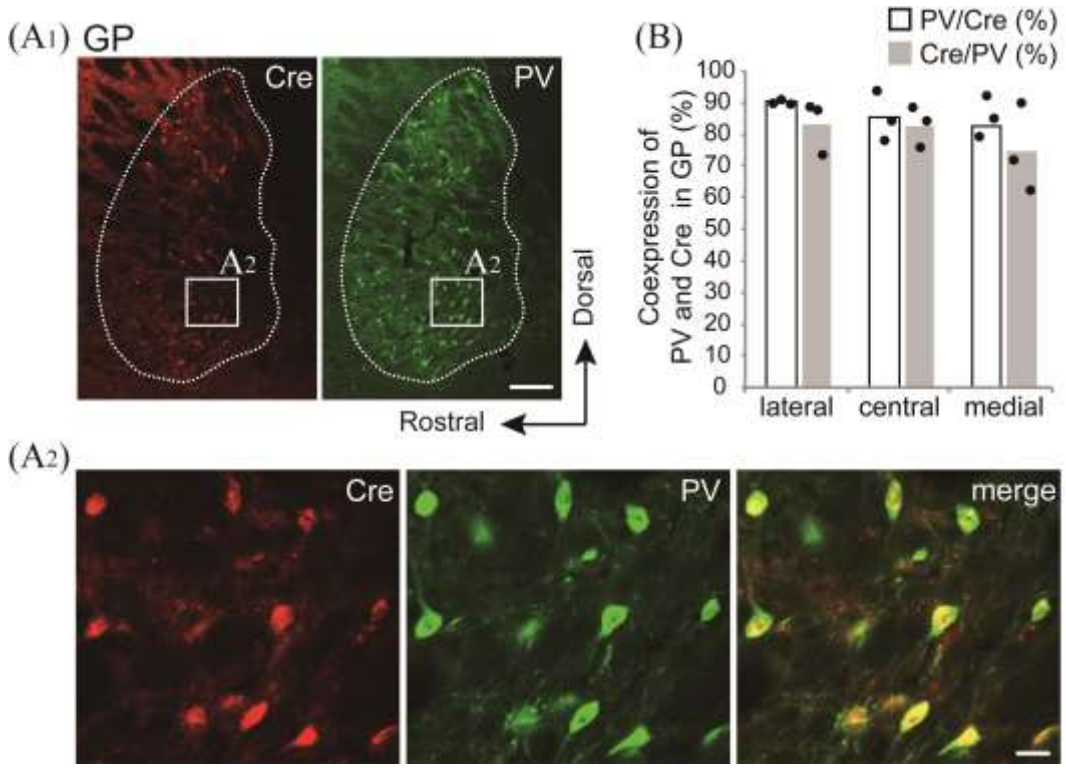

Fig. 4 Double immunofluorescence labeling for Cre and parvalbumin (PV) immunofluorescence in the globus pallidus (GP) of PV-Cre rats

Low- (A1) and high-magnification images (A2) showing Cre (AF594) and PV (AF488) double immunofluorescence labeling in the GP of PV-Cre rats. A2 is high-magnification image of the GP from the boxed area shown in A1. Note that most of Cre immunopositive neurons showed PV immunoreactivity. (B) Proportions of Cre-GP neurons co-expressing PV (open bars) and proportions of PV-GP neurons co-expressing Cre (filled bars) in different latero-medial subdivisions of the GP (N = 3 rats; shown as dots). Photos were taken with an epifluorescent microscope (BX-61, Olympus, Tokyo, Japan) under the conditions described in the Materials and Methods. Scale bars: (A1), 200 μm; (A2), 25 μm.

3. 2. Neuronal subpopulations of GP

STN-projecting cells in the GP, which are prototypic neurons, are known to express PV and/or Lhx6 (Flandin et al. 2010; Nóbrega-Pereira et al. 2010; Mastro et al. 2014; Abdi et al. 2015; Dodson et al. 2015; Hernandez et al. 2015). Given the continued debate regarding the proportion and molecular composition of PV neurons in the GP (Flandin et al. 2010; Nóbrega-Pereira et al. 2010; Mastro et al. 2014; Abdi et al. 2015; Dodson et al. 2015; Hernandez et al. 2015), we used double or triple immunofluorescent staining to further evaluate whether PV immunoreactive neurons might exhibit other molecular markers specific for GABAergic neuron subpopulations; the results of this evaluation are summarized in Fig. 5C. The neuronal marker NeuN was used to label all GP neurons (Figs. 5A and C); and as in previous reports, 38.8 ± 5.51% and 57.31 ± 6.57% of GP neurons expressed PV and Lhx6, respectively (Figs. 5A and C, N = 16,531 cells from 27 sections in five rats). We determined that 57.05 ± 12.9% of PV neurons co-expressed Lhx6, whereas 44.37 ±8.1% of Lhx6 neurons co-expressed PV (Figs. 5A, B and D). Co-expression of PV and FoxP2 was negligible (0.35 ± 0.37%, Figs. 5B and 5D). In addition, $Lhx6^{+}$/ PV^{-} neurons were more abundant in GP ventral area than the dorsal area (Fig. 6). Above results suggested that PV neurons could be further divided into $PV^{+}/Lhx6^{+}$ and $PV^{+}/Lhx6^{-}$and less than half of $Lhx6^{+}$ neurons expressed PV in our experiment (but see Abdi et al. 2015). Therefore using the PV-Cre rat line, we could select only PV-GP neuronal population among prototypic neurons.

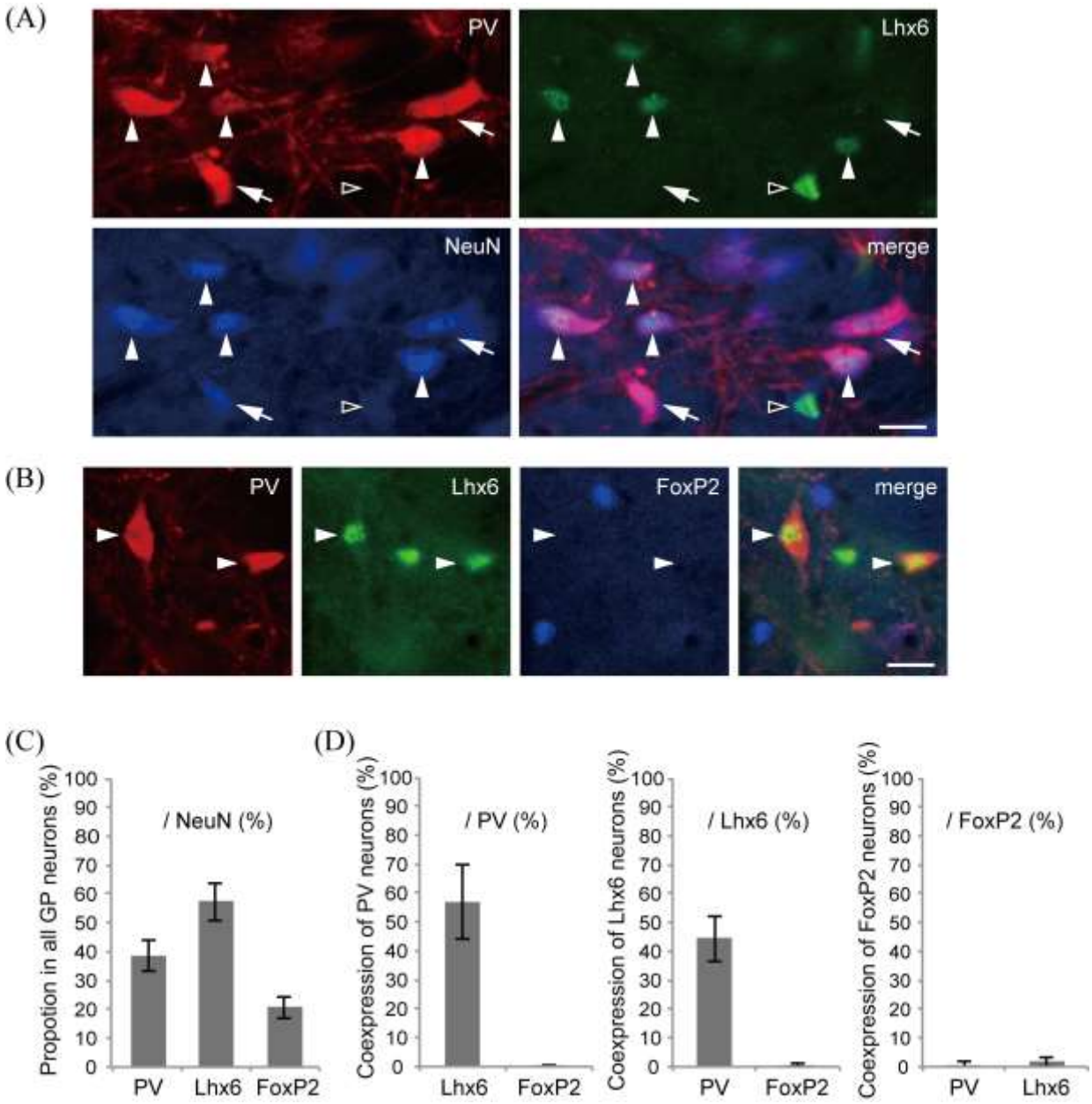

Fig. 5 Immunohistochemical identification of the globus pallidus (GP) neuron classes

High-magnification image of the GP, showing triple immunofluorescence labeling for parvalbumin (PV; red), Lhx6 (green), and NeuN (blue) shown in (A) and PV (red), Lhx6 (green), and FoxP2 (blue) in (B). (A) $PV^+/Lhx6^+$ (arrowheads), $PV^+/Lhx6^-$ (arrows) and $PV^-/Lhx6^+$ (black arrowheads) immunoreactive neurons were observed. (B) In contrast, no FoxP2 immunoreactivity was observed in PV- or Lhx6-immunoreactive neurons. Scale bars: 25 μm. (C) Expression frequencies of given molecular markers (data pooled across the lateral, central, and medial GP; 5 rats, 7 hemispheres, 27 sections, 16,531 cells) in all GP neurons, defined using the NeuN. (D) Expression frequencies of given molecular markers (data pooled across lateral, central, and medial GP) in each immunohistochemical GP neuron class, defined using corresponding molecular markers. Note that PV and FoxP2 were expressed in a largely non-overlapping manner. In contrast, considerable overlap was observed between Lhx6 and PV (Lhx6/ PV = 57.1 ± 12.9%; PV/ Lhx6 = 44.4 ± 8.1%).

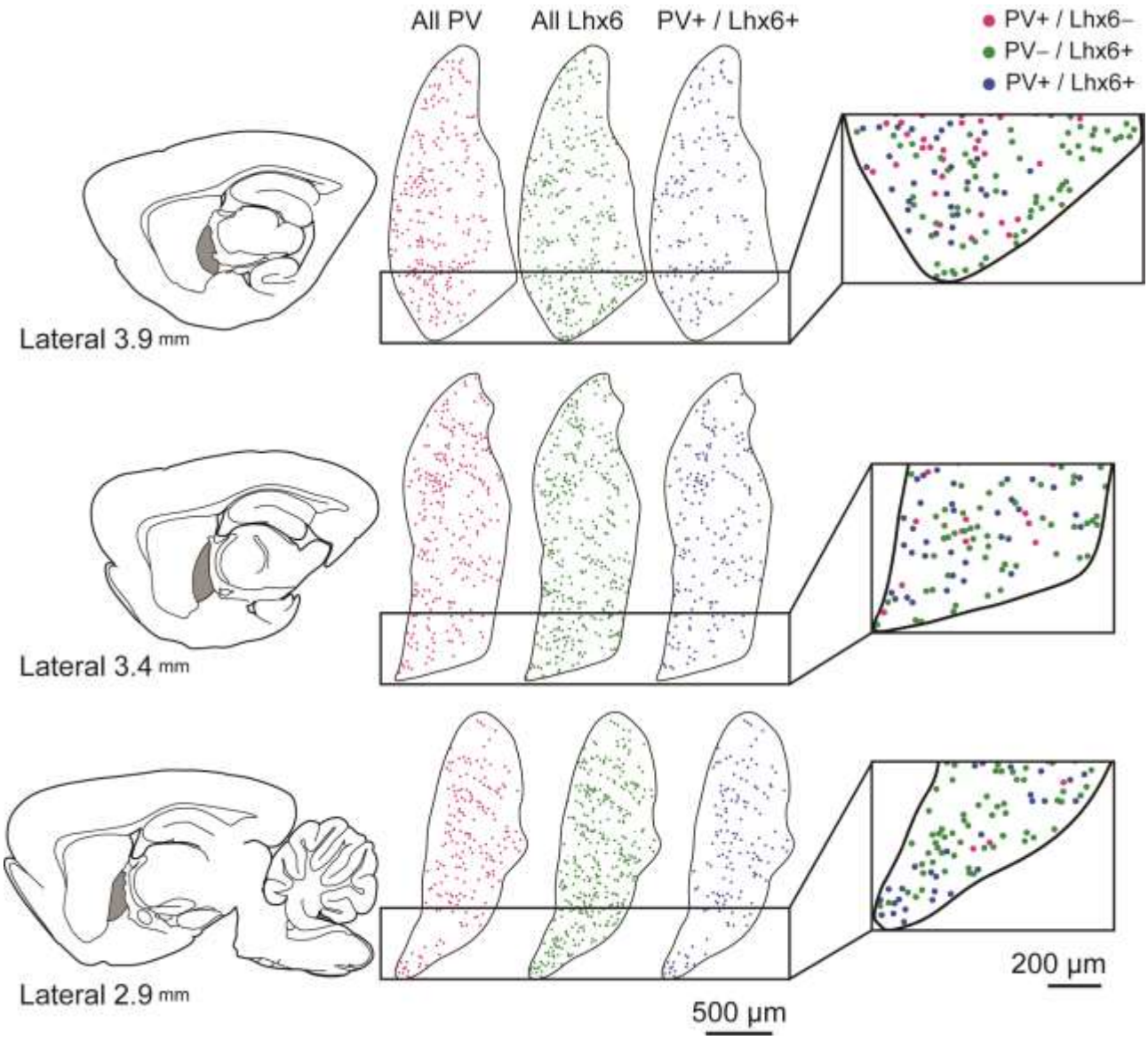

Fig. 6 Spatial distribution and co-expression of PV and Lhx6 in the GP neurons.

Immunohistochemically identified PV^+ (red dot), $Lhx6^+$ (green dot), and $PV^+/Lhx6^+$ (blue dots) neurons were plotted in three sagittal planes. The magnified views of the ventral region are shown in the rightmost column. In the rightmost column, $PV^+/Lhx6^-$ (red dot), $PV^-/Lhx6^+$ (green dot), and $PV^+/Lhx6^+$ (blue dots) neurons are indicated. Distribution of them was likely to be unbiased in the GP, however, $Lhx6^+/PV^-$ neurons (green) were outstanding in the ventral region of the GP at LM2.9-3.9 mm.

Table 3. Co-expression of molecules in the GP of wild type Long Evans and PV-Cre rats

population	co-expressed with	# of sections	Long Evans	PV-Cre
/ PV neurons	Lhx 6	18	41.73 ± 9.37%	47.01 ± 5.92%
	FoxP2	18	0.35 ± 0.34%	0.35 ± 0.60%
/ Lhx6 neurons	PV	18	56.02 ± 15.10%	58.09 ± 11.10%
	FoxP2	9	0.64 ± 0.78%	0.83 ± 0.16%
/ FoxP2 neurons	PV	18	0.58 ± 0.54%	1.18 ± 2.04%
	Lhx 6	9	1.34 ± 1.64%	1.99 ± 0.88%

3. 3. Projection of axon fibers from PV neurons in the GP to the SN

The specificity of Cre expression in the transgenic rats was further examined via Cre/loxP-mediated tdTomato expression after AAV injection into the GP (Figs. 7A and 7C). Since AAV injection could not cover whole area of the GP, hereafter, we analyzed only neurons infected with AAV, namely, expressing tdTomato fluorescence. TdTomato fluorescence from AAV-infected neurons colocalized strongly with PV immunoreactivity in the GP (Fig. 7D, 89.0 ± 4.7%, number of infected cells = 825 from 20 sections in five rats) and the axons of these neurons were mainly distributed in the STN, EP, and SN but rarely in the striatum (Fig. 7B).

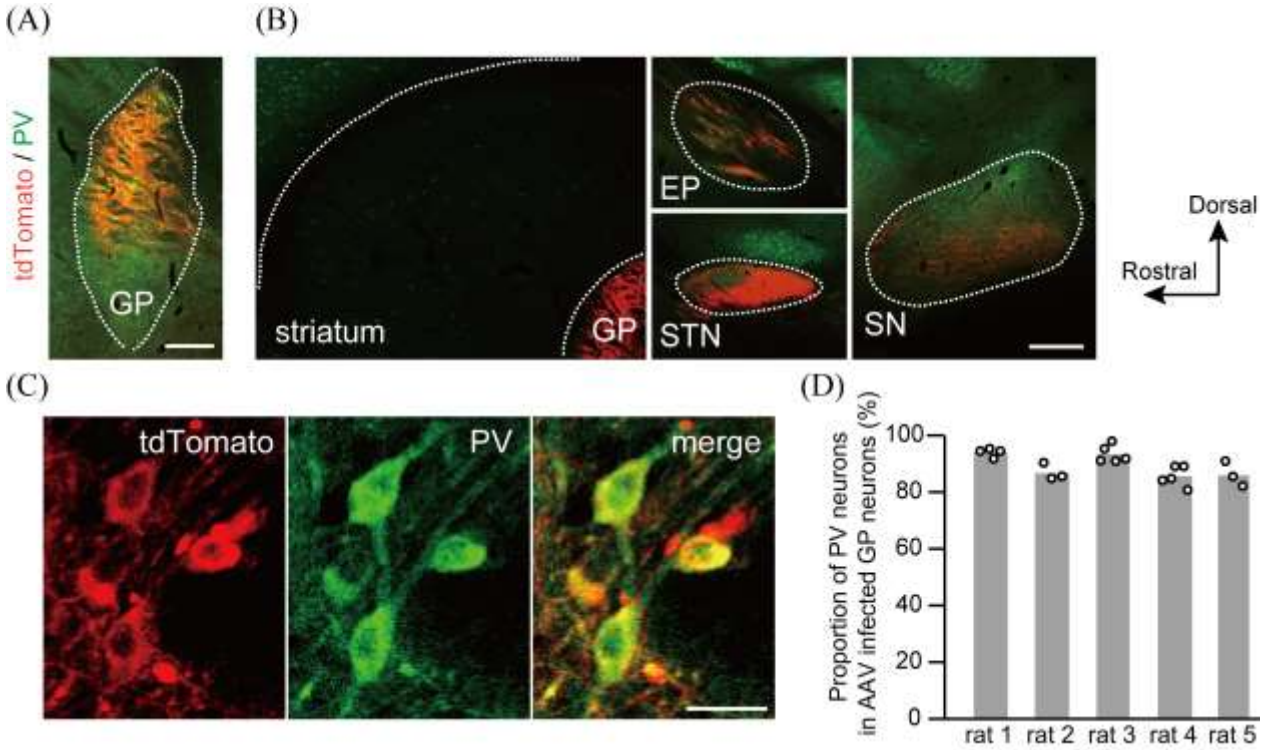

Fig. 7 Efficient labeling of PV neurons using AAV vector encoding loxP in PV-Cre rats.

(A) Low-magnification image displaying the viral injection site in the globus pallidus (GP). Scale bar: 500 μm. (B) Fluorescent labelling of PV-GP projections to basal ganglia output nuclei (entopeduncular nucleus [EP], substantia nigra [SN]), subthalamic nucleus (STN) and striatum. Note the faint immunofluorescence in the striatum relative to the EP, SN, or STN under the same exposure condition. Scale bar: 500 μm. (C) High-magnification images displaying infected neurons at the viral injection site in the GP. Note that most infected neurons (red in the left panel) coexpressed PV (green in the middle panel and yellow in the merged panel). Scale bar: 20 μm. (D) Five filled bars indicate the proportion of PV neurons in GP neurons infected with AAV of five rats, respectively. Circles represent data from individual sections.

In addition, Lhx6+/PV− neurons were rarely found in AAV infected GP neurons (Fig. 8). Taken together, Cre dependent AAV infection was highly selective for PV neurons. In the examined cases, no PV somata were labeled via retrograde infection in the striatum, EP and SN (Fig. 9), suggesting that most of the axons in the SN originated from PV-GP neurons. The dense distribution of tdTomato-fluorescent axons in the STN and limited presence in striatum in the present study was compatible with an understanding of PV-GP neurons as prototypic neurons (Abdi et al. 2015).

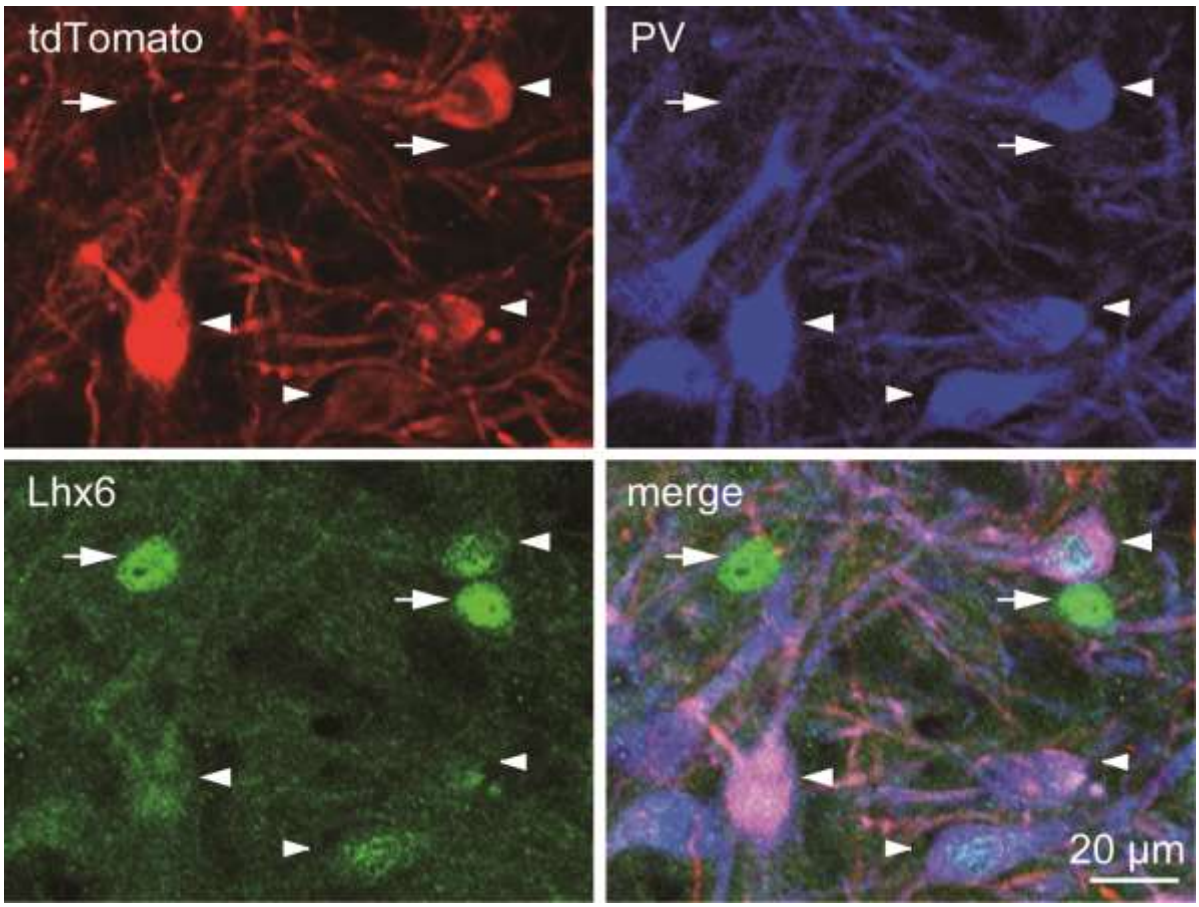

Fig. 8 tdTomato fluorescence, PV (blue) and Lhx6 (green) immunoreactivities in parvalbumin (PV)–Cre rats at 2 weeks after viral injection.

High-magnification images displaying the viral injection site in the globus pallidus. Arrowheads indicated the $Lhx6^{+}/PV^{+}$ neurons. Note that $Lhx6^{+}/PV^{-}$ neurons (arrows) were rarely infected. Photos were taken with a confocal microscope (FV-1200, Olympus, Tokyo, Japan) under the conditions described in the Materials and Methods. Scale bars: 20 μm.

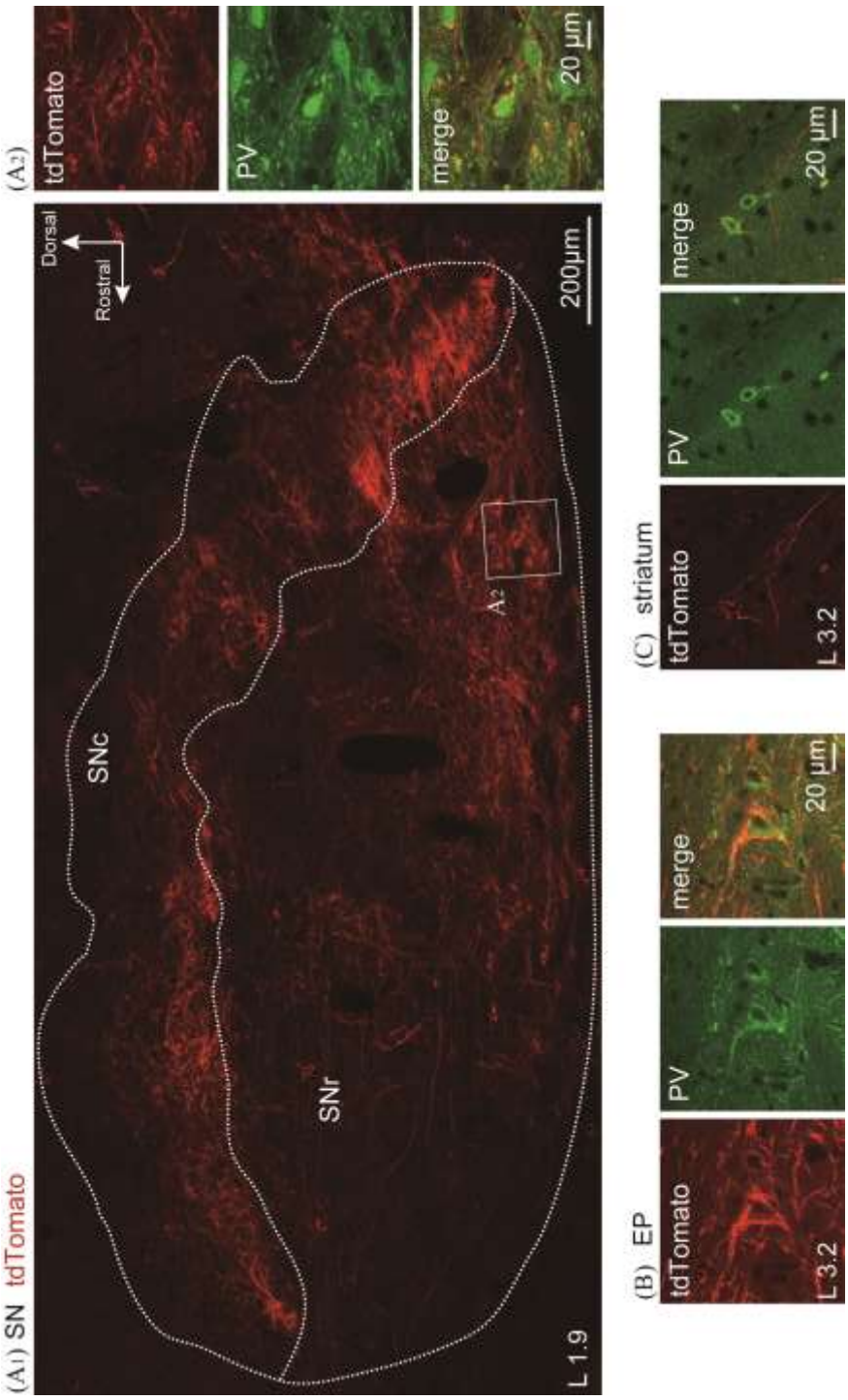

Fig. 9 AAV vector used here did not label neurons retrogradely.

Fluorescent images of the SN (A), EP (B), and striatum (C) of a rat after AAV injection into the GP. TdTomato labelled axons from PV-GP neurons were observed in all images. Importantly, no retrograde labelling of PV neurons was observed. A neuron-like shape of fluorescence was investigated at some locations in SNr (A2) and EP (B), however, magnified views combined with PV immunoreactivity (green) revealed that these pseudo-cell like fluorescence was not AAV-infected neurons. Actually they were unlabeled neurons which were surrounded by dense PV-GP axons. (C) In striatum, no such image was observed due to relatively weak PV-GP projections. Photos were taken with a confocal microscope (FV-1200, Olympus, Tokyo, Japan) under the conditions described in the Materials and Methods.

In the SN, SNcd and SNcv contain dopamine neurons known to express tyrosine hydroxylase (TH; Fig. 12C), and in the present study, this SNc division was always precisely defined via TH-immunostaining (Fig. 11A). Populations of PV-GP axons were not distributed uniformly but with clear topographical organization in the SN (Figs. 10; sample ID is described as a – e). We found common features of PV-GP axon distribution in relation to the LM axis of the SN. In the most lateral SN (LM > 2.9 mm), PV-GP axons were only faintly observed (data not shown). At LM 2.1 – 2.8 mm, all axons of PV-GP neurons were oriented toward the SNr and arborized loosely as long collaterals with terminations (Figs. 10, 11 and 17). In contrast, at LM 1.55 – 2.4 mm, PV-GP axons formed relatively dense axon varicosities with many terminal boutons in the border region between the SNcd and SNr, corresponding area II and III in Fig. 12D (Figs. 10-13 and 17), as well as in the SNcv (Figs. 10b-e). Since both the TH- and PV-immunoreactive dendrites intermingled in the border region between the SNcd and SNr, we quantified the PV-GP axonal boutons in the region (see Materials and Methods, Fig. 2, 10-13).

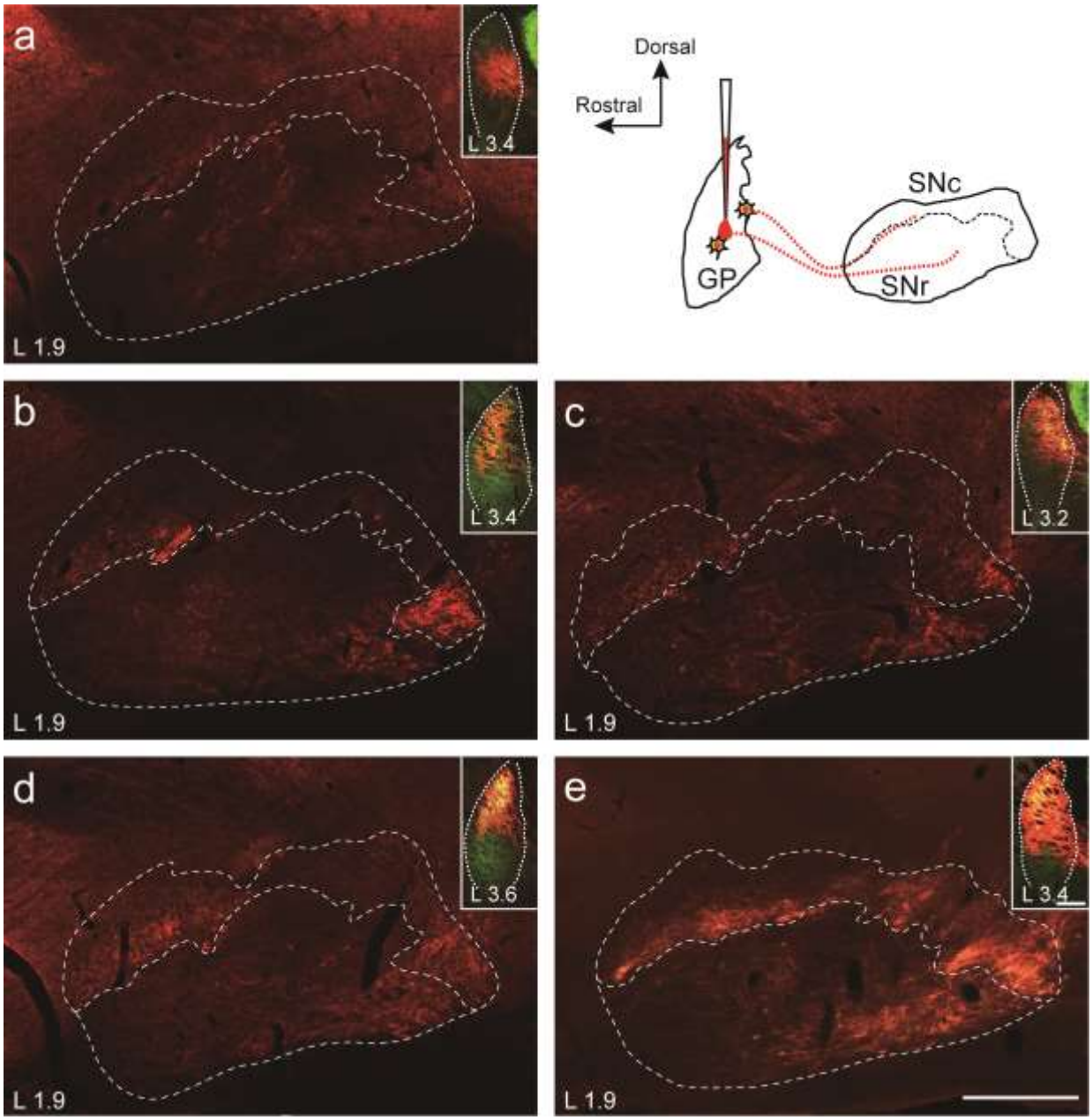

Fig. 10 Fluorescent images of axons in the substantia nigra pars compacta (SNc) and reticulata (SNr) originated from parvalbumin (PV)–globus pallidus (GP) neurons

Five confocal images of axons in the SN (cases a–e, sections at 1.9 mm lateral from the midline (L1.9)) issued from PV–GP neurons. Fluorescent images in the upper right corner display the virus injection centers in the GP. In 4 of 5 cases, the injection center was located at 3.4 mm lateral from the midline (L3.4) and the remaining at L3.6. PV immunoreactivity was overlaid in the insets (green). The contours of SN and the border between SNc and SNr were drawn in dotted lines using simultaneous immunostaining for TH and PV. For the SN images, PV and TH fluorescence was omitted to make detailed PV-GP axon images clearer. Note that dense boutons of PV-GP axons emerged in the border region between the SNc and SNr. Photos were taken with an epifluorescent microscope (BX-61, Olympus, Tokyo, Japan) under the conditions described in the Materials and Methods. The imaged sagittal plane of the SN was taken from the sections containing the densest PV-GP axons. Scale bars in GP and SN: 500 μm.

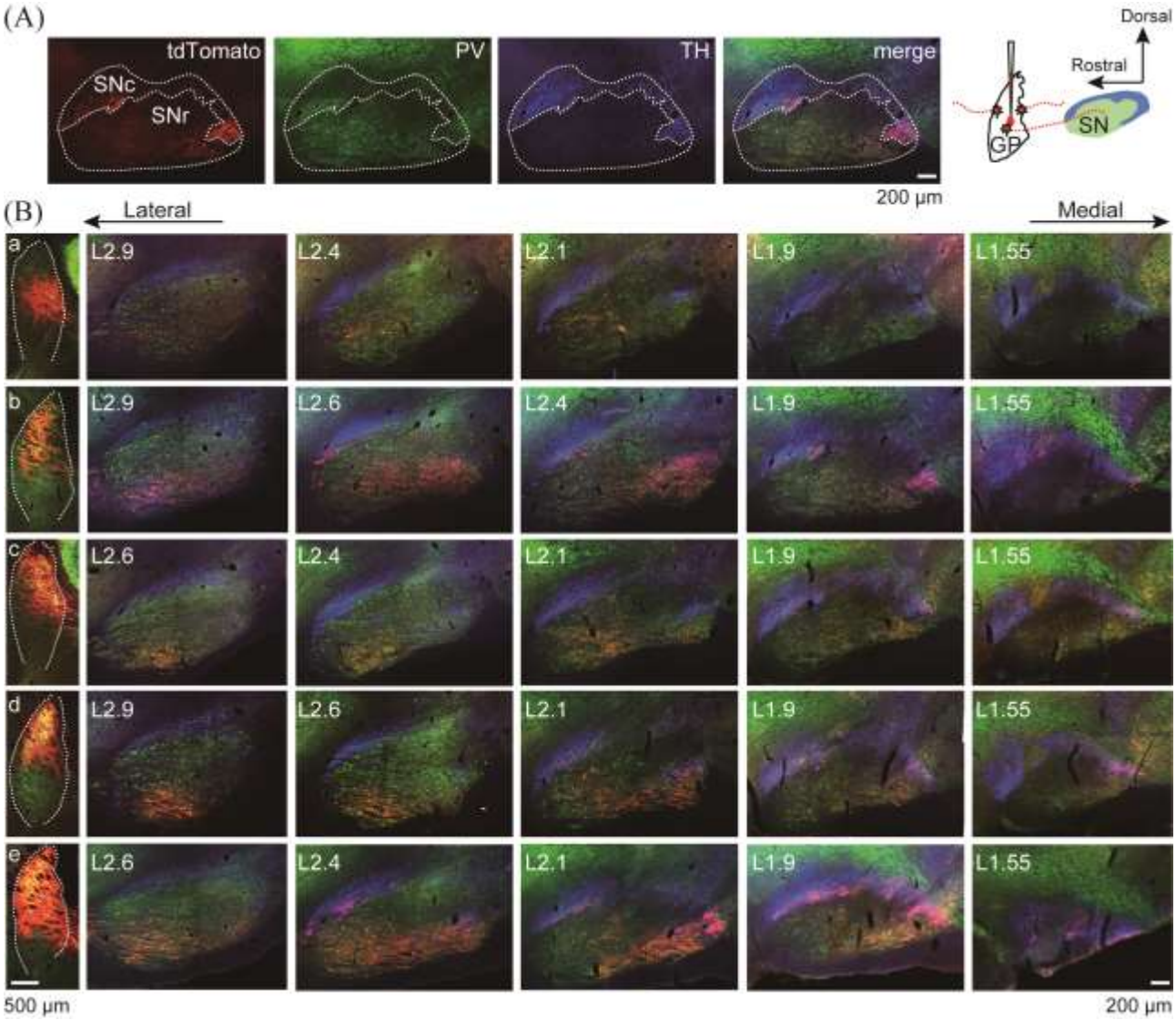

Fig. 11 Fluorescent images of axons from parvalbumin (PV)–globus pallidus (GP) neurons in the substantia nigra pars compacta (SNc) and reticulata (SNr)

(A) Overlay (the most right) of PV–GP axons (red), tyrosine hydroxylase (TH, blue) and PV (green) immunofluorescence in case b. Using TH and PV immunoreactivity SNc and SNr were identified. (B) Fluorescent images of axons from PV–GP neurons in the SN from 5 PV-Cre rats (cases a–e). Fluorescent images in the left column display the virus injection sites in the GP. Five latero-medial planes of SN images are arranged from left (the most lateral plane) to right (the most medial plane), ranged from 1.55 to 2.9 mm. Note that dense boutons of PV-GP axons emerged in the border region between the SNc and SNr. See also Fig. 12. Photos were taken with an epifluorescent microscope (BX-61, Olympus, Tokyo, Japan) under the conditions described in the Materials and Methods. Scale bars: 500 μm in GP and 200 μm in SN.

Qualitatively, PV-GP axons were significantly dense in the ventral part of SNcd corresponding area II in Fig. 12D (Figs. 12A and 12B, Friedman test, $p<0.001$). It is notable that the density of the boutons showed preference to the ventral part (area II in Fig. 12D) rather than dorsal part (area I in Fig. 12D) of SNcd (Figs. 12A and 12B, Friedman test, Bonferroni's post-hoc multiple-comparison, area I (dorsal part of SNc) vs. area II (ventral part of SNc): $p<0.01$). In addition, it is further notable that the density indicated a preference for the ventral part of SNcd(area II in Fig. 12D), where TH somata exist, rather than the dorsal part of SNr (area III in Fig. 12D), where GABAergic somata exist (Figs. 12A and 12B, Friedman test, Bonferroni's post-hoc multiple-comparison, area II (ventral part of SNc) vs. area III (dorsal part of SNr): $p<0.05$). Because PV neurons are considered as '"basket" cells that prefer to make synaptic contacts on the cell bodies of the target cells, we next quantified whether axonal boutons were localized around the surfaces of various types of neurons in the border region. After normalizing the estimated distances between the axonal boutons and cell centers as described in the Materials and Methods, we found that the density of the axonal boutons around a TH positive cell was significantly higher near the edge of a cell body (Fig. 14, Wilcoxon rank-sum test, a: $p <0.001$, N = 23 cells; b: $p <10^{-20}$, N = 124; c: $p <10^{-13}$, N = 80; d: $p <10^{-10}$, N = 70; e: $p <10^{-20}$, N = 146; f: $p <0.05$, N = 24; g: $p <10^{-13}$, N = 79; h: $p <10^{-9}$, N = 95; i: $p <10^{-6}$, N = 47). Similarly, for PV-positive cells, the axonal boutons were localized near the edge (Fig. 14, Wilcoxon rank-sum test, a: $p <0.05$, N = 9; b: $p <10^{-4}$, N = 20; c: p = not assigned (NA), N = 4; d: $p <0.01$, N = 17; e: $p <0.05$, N = 13). We also found that the density of the axonal boutons around cholecystokinin (CCK)- and calretinin (CR)-positive cells was

significantly higher near the edge of a cell body (Fig. 16, Wilcoxon rank-sum test, g: $p < 0.001$, $N = 18$; h: $p < 10^{-6}$, $N = 65$). For Calbindin (CB)- and nitric oxide (NOS)-positive cells, boutons were rarely observed in the regions that we examined (Fig. 12, f (CB): $N = 4$; i (NOS): $N = 0$).

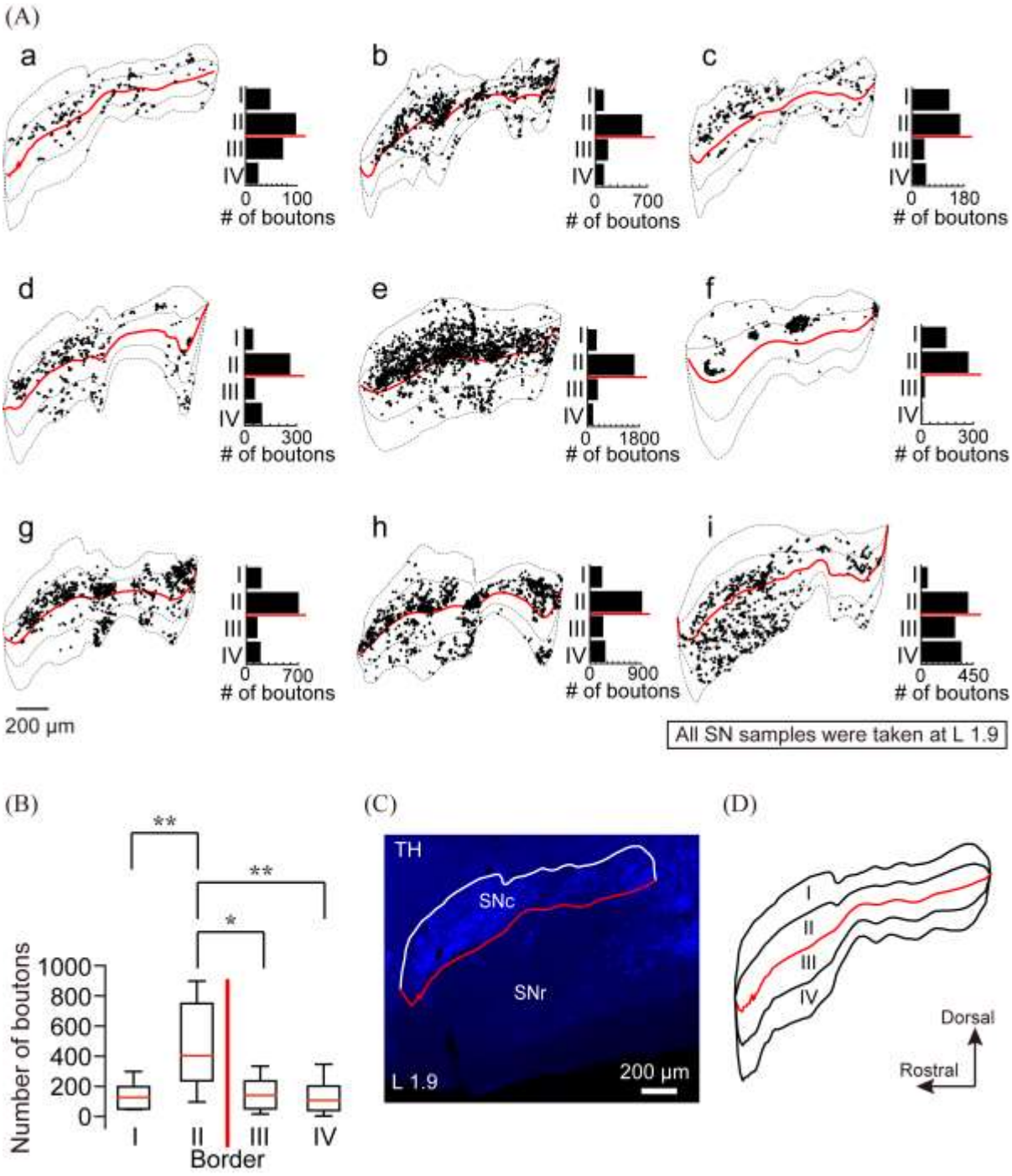

Fig. 12 Spatial distribution of PV-GP axon boutons near the border between substantia nigra pars compacta (SNc) and pars reticulata (SNr)

(A) Nine panels show the spatial distribution of PV-GP axon boutons near the border between SNc and SNr for each sample (sections at 1.9 mm lateral from the midline (L1.9)). The sample ID (a–i) was described at the top. The dot indicates an identified bouton. The analyzed region was divided into four dorso-ventral areas: I (dorsal part of SNc dorsal tier (SNcd), II (ventral part of SNcd), III (dorsal part of SNr in the analyzed region) and IV (ventral part of SNr in the analyzed region), as shown in (C) and (D). See also Fig, 2. Red line indicates the SNc/SNr border. At the right side, the total number of boutons in each area was shown. Note PV-GP boutons were highly concentrated in area II, the ventral part of SNcd in all cases. (B) The number of boutons across all samples, as a function of four areas (red horizontal lines: median; boxes: the first and third quartiles; bars:

minimum and maximum values). Friedman test and Bonferroni's post-hoc multiple-comparison revealed significantly larger number of boutons were located in area II (*: $p < 0.05$, **: $p < 0.01$). The red vertical line illustrates the border between SNc and SNr.

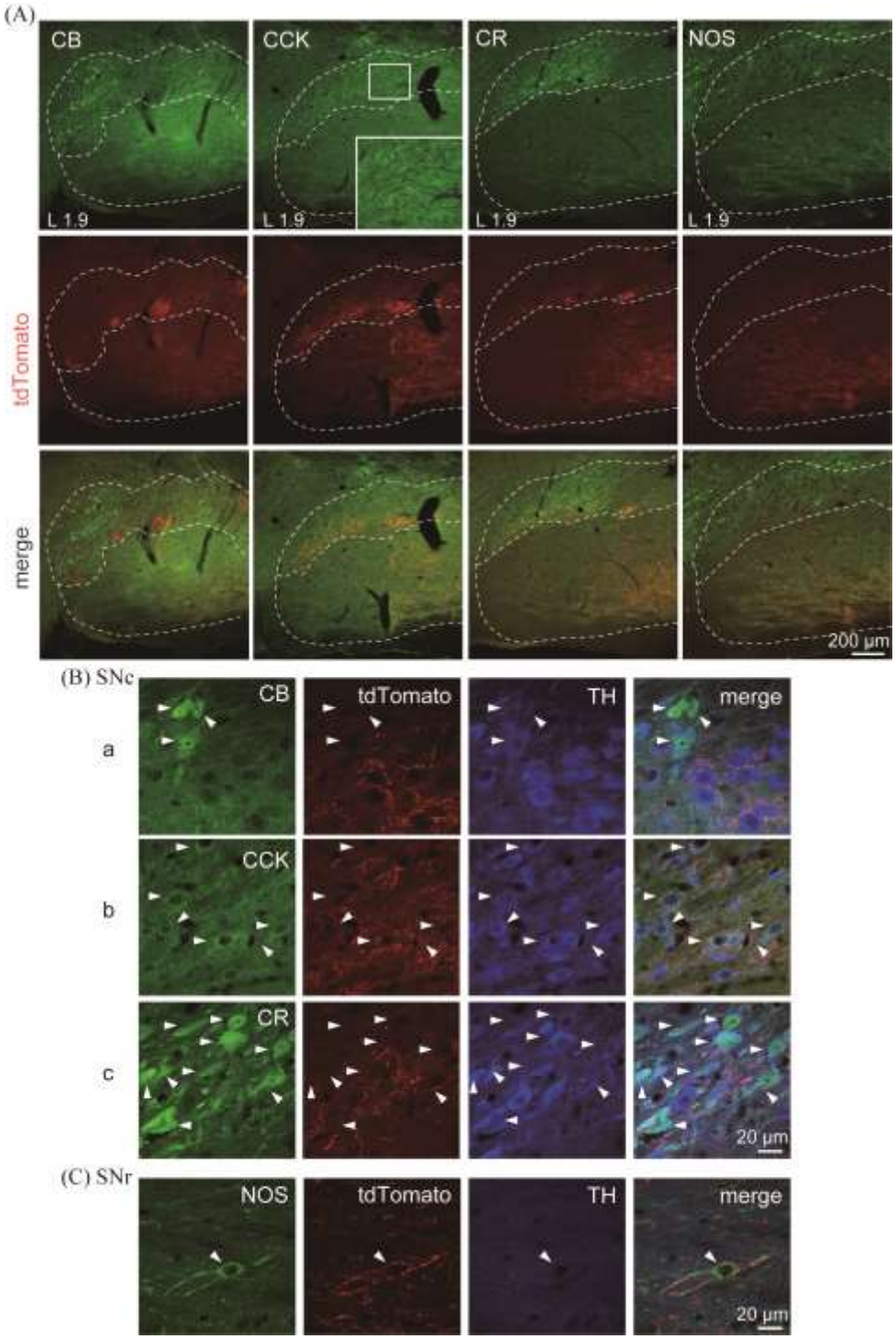

Fig. 13 Fluorescent images of CB, CCK, CR or NOS-positive cell body and axons from PV-GP neurons in the SN

Overlay of PV–GP axons (red), CB, CCK, CR or NOS (green) immunofluorescence in SN (A), SNc (B) and SNr (C). Note that PV-GP axons formed basket-like appositions with CCK (b) and CR (c) but CB (a) immunoreactive somata in the SNc and with NOS (C) immunoreactive soma in the SNr. PV-GP axons in the border region between the SNc and SNr formed basket-like appositions with CCK and CR somata. Photos were taken with a confocal microscope (FV-1200, Olympus, Tokyo, Japan) under the conditions described in the Materials and Methods. Scale bar: low magnification, 200 μm; high magnification, 20 μm.

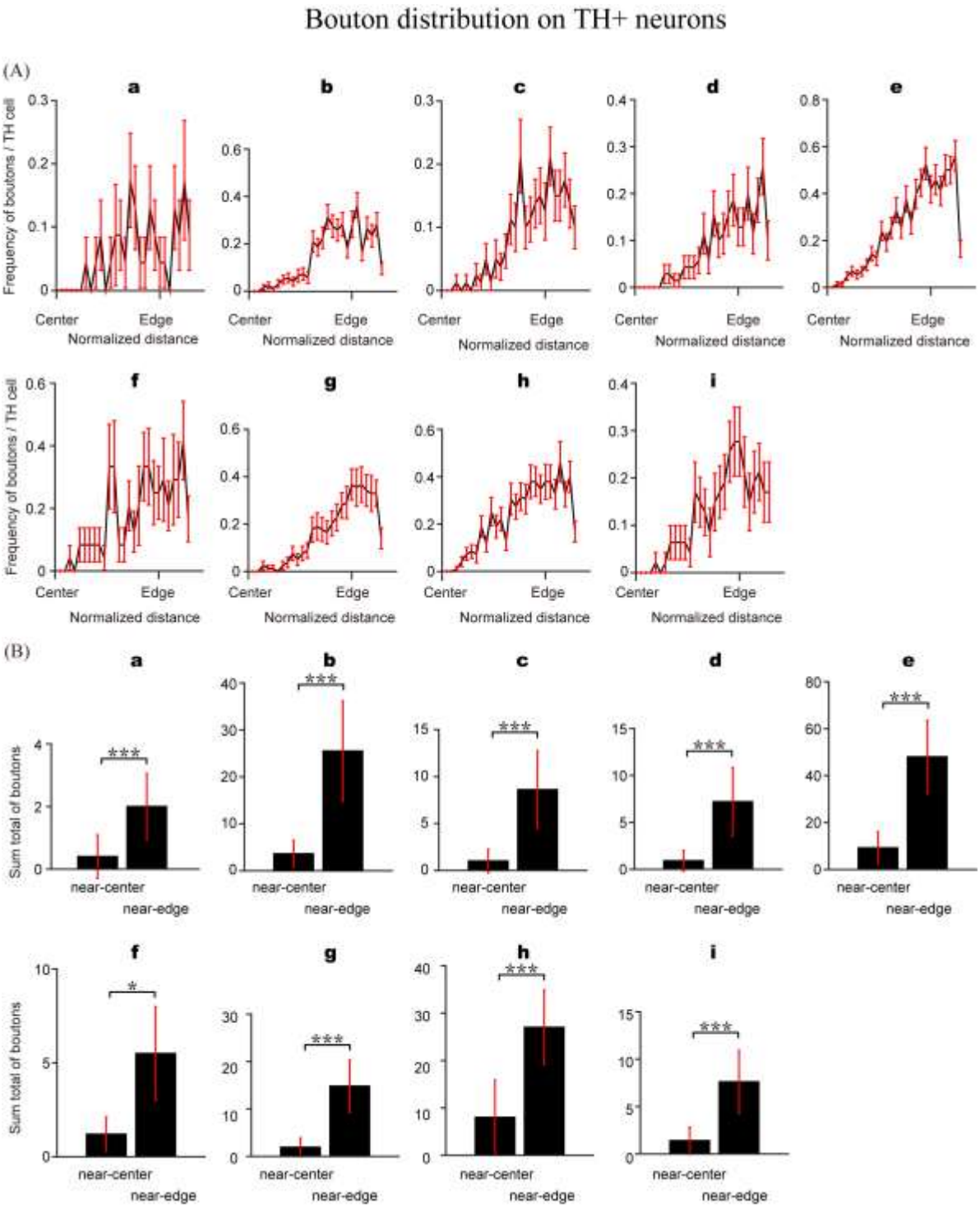

Fig. 14 Estimated distances between the centers of the TH-positive cell bodies and PV-GP boutons

Sample IDs are indicated in the topmost section, which are the same as those in Fig. 11. (A) Average frequency of the number of boutons per TH-positive cell as a function of the normalized distance between the cell center and edge. Red bars indicate standard errors of the mean. (B) Bar graph shows the sum total of boutons for each cell within the near-center and near-edge regions, respectively. The borderline between the cell center and edge is set at the midpoint. Red bars indicate standard deviations. Wilcoxon rank-sum test, *: $p<0.05$, ***: $p<0.001$.

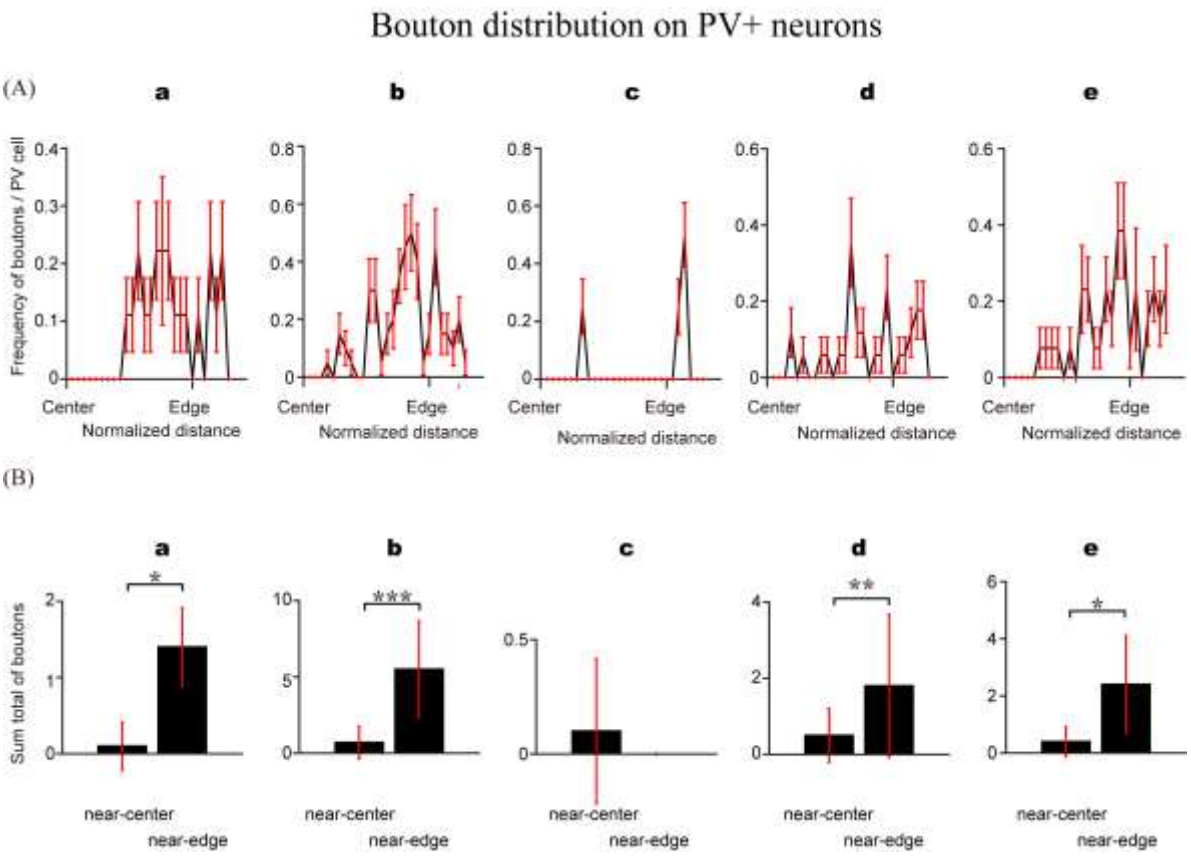

Fig. 15 Estimated distances between the centers of the PV-positive cell bodies and PV-GP boutons

Sample IDs are indicated in the topmost section, which are the same as those in Fig. 6. (A) Average frequency of the number of boutons per PV-positive cell as a function of the normalized distance between the cell center and edge. Red bars indicate standard errors of the mean. (B) Bar graph shows the sum total of boutons for each cell within the near-center and near-edge regions, respectively. The borderline between the cell center and edge is set at the midpoint. Red bars indicate standard deviations. Wilcoxon rank-sum test, *: $p<0.05$, **: $p<0.01$, ***: $p<0.001$.

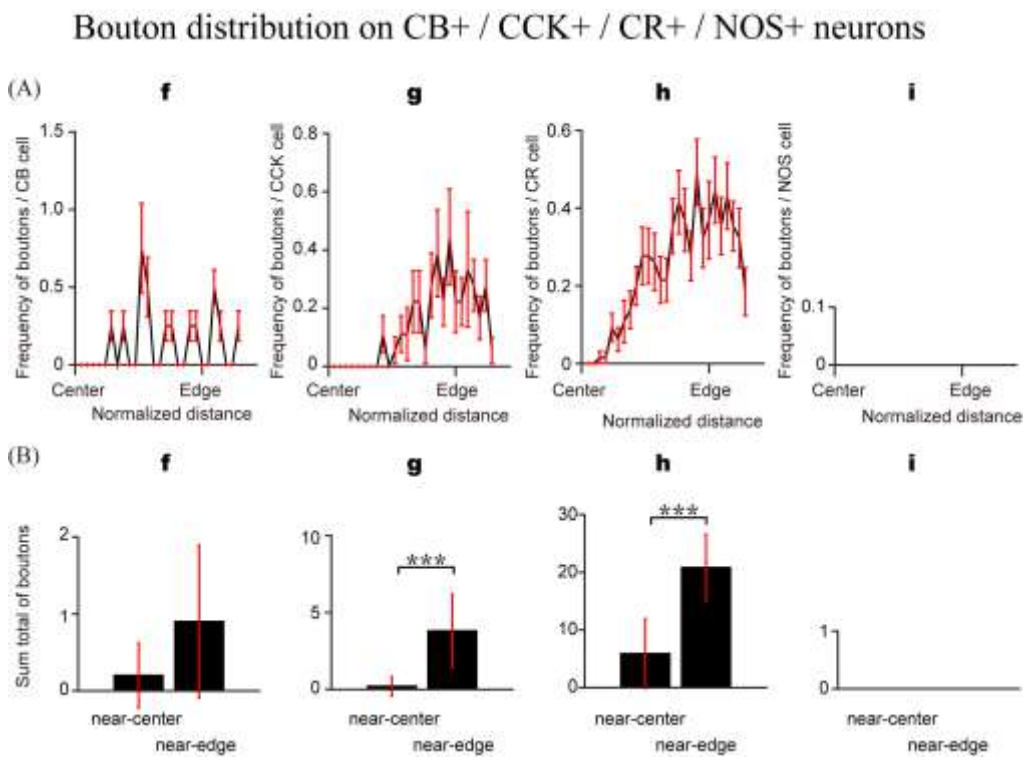

Fig. 16 Estimated distances between the centers of the CB, CCK, CR or NOS-positive cell bodies and PV-GP boutons

Sample IDs are indicated in the topmost section, which are the same as those in Fig. 11. (A) Average frequency of the number of boutons per CB (f), CCK (g), CR (h) or NOS (i) -positive cell as a function of the normalized distance between the cell center and edge. Red bars indicate standard errors of the mean. (B) Bar graph shows the sum total of boutons for each cell within the near-center and near-edge regions, respectively. The borderline between the cell center and edge is set at the midpoint. Red bars indicate standard deviations. Wilcoxon rank-sum test, ***: $p<0.001$. Since for CB and NOS - positive cells, few boutons were located around the cell body, statistical test could not be performed.

3. 4. PV-GP neurons innervate the dopaminergic SNc and GABAergic SNr neurons

To further support the concept of a closed apposition as a potential synapse, it is necessary to label post-synaptic structures. Therefore, we introduced immunofluorescent labeling for gephyrin, one of the GABAergic post-synaptic markers. PV-GP somatic appositions with TH somata were frequently observed in the border region between the SNcd and SNr at LM 1.5–2.4 mm (Figs. 10-12) and the SNcv at LM 1.5–2.1 mm (Figs. 10-12), whereas similar terminals surrounding PV-positive cell bodies were scattered in the SNr at LM 1.9–2.9 mm (Figs. 11 and 15). Orthogonal views of triple immunofluorescence images further indicated that PV-GP axon terminals were in close apposition with gephyrin on TH- or PV- immunoreactive dendrites and cell bodies (arrowheads in Figs. 18A and B). Because gephyrin serves as a cytoskeletal anchor in inhibitory synapses and provides a scaffold for other postsynaptic proteins, GABA, and glycine receptors, such appositions are probably the sites of inhibitory synapses. According to previous reports (Smith and Bolam 1990b; Bevan et al. 1996), such potential synapses were also observed on proximal dendrites to the soma (Fig.18B). In the next section, we demonstrate that those potential synapses were actually functional GABAergic synapses.

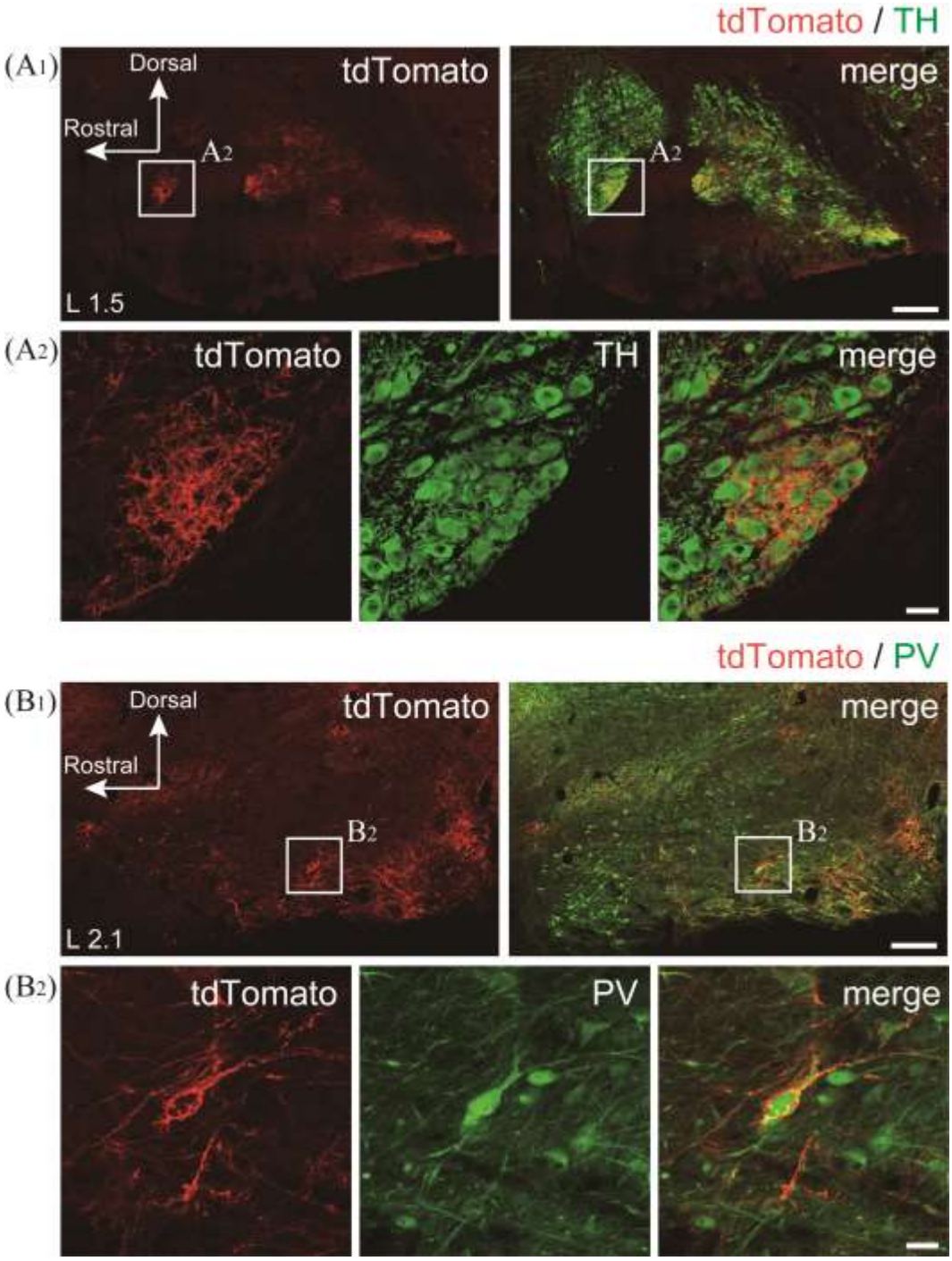

.Fig. 17 PV-GP neurons formed large and dense axon varicosities in the ventral part of the SNcd, and SNr.

(A1) In SNc, PV-GP axons (labelled by tdTomato) were not distributed in whole area, rather preferentially observed at the ventral part of SNcd. (A2) The magnified view of the area shown in the A1 (white rectangle). PV-GP boutons were highly concentrated in a small region providing dense basket-like terminal structures onto TH neurons (green). (B1) In SNr, PV-GP axons arborized relatively loosely into long collaterals in a wide area of SNr. (B2) The area shown in the B1 was magnified. Locally PV-GP axons formed basket-like appositions with PV somata and dendrites (green). Photos were taken with a confocal microscope (FV-1200, Olympus, Tokyo, Japan) under the conditions described in the Materials and Methods. Scale bar: low magnification, 200 μm; high magnification, 25 μm.

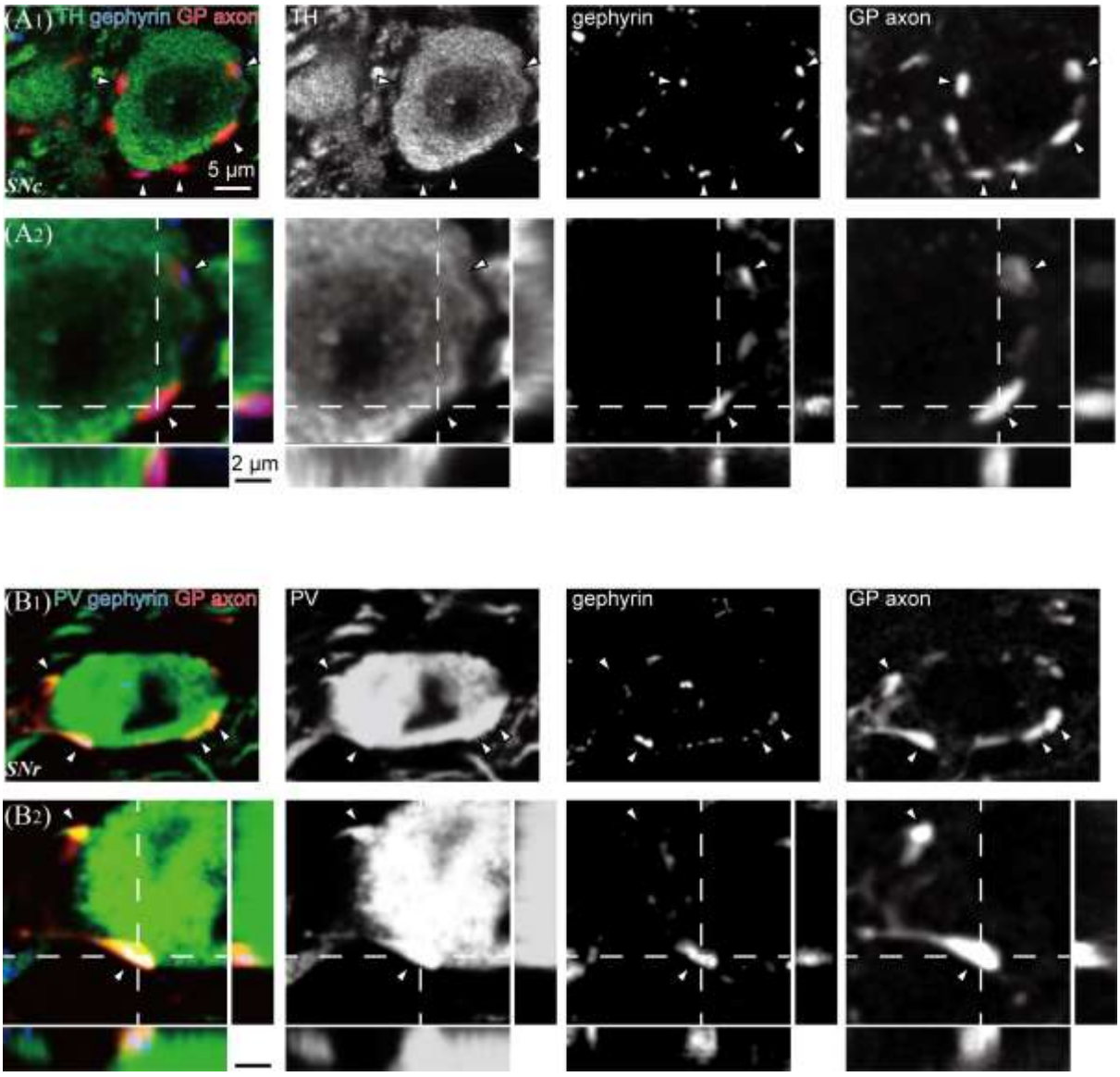

Fig. 18 Somatic apposition on substantia nigra (SN) neurons by parvalbumin (PV)-globus pallidus (GP) axon terminals associated with the GABAergic post-synaptic marker, gephyrin

(A) Triple fluorescence images of tyrosine hydroxylase (TH, green), gephyrin (blue), and PV-GP axon structures (red) in the SN pars compacta (SNc). (A1) PV-GP axon terminals formed close appositions on TH soma and dendrites. Gephyrin staining closely located to these structures (arrowheads). (A2) Magnified views of two of the somatic appositions shown in A1 (the rightmost 2 arrowheads). Note that the TH soma surface, gephyrin, and PV-GP terminals were co-localized in a single confocal plane; orthogonal views are also presented at the dotted line plane. (B) Triple fluorescent images of a PV (green) neuron in the SN reticulata (SNr). (B1) Three somatic and one dendritic apposition can be observed (arrowheads). (B2) Magnified views of a somatic (lower) and dendritic (upper) appositions, corresponding to the leftmost 2 appositions in B1. Note that PV was expressed not only in a PV neuron in the SNr, but also in PV-GP axon structures. The scale bars in (A) are also applied to (B)

3. 5. PV-GP neurons inhibit the dopaminergic SNc neurons

Seven PV-Cre rats were infected with AAV-FLEX-rev-ChR2-tdTomato to induce channel rhodopsin 2 (ChR2) expressions in PV-GP neurons and their axon terminals. Using *in vitro* slice preparation, being similar to the perfusion section data in Fig. 10, dense tdTomato-labeled GP axon terminals in the SNc were also observed in in vitro slices. Whole-cell patch clamping was used to record the SNc neurons surrounded by those PV-GP terminals (N = 11 cells), as well as 3 SNr neurons to confirm whether SNc neurons possessed characteristic membrane properties. As shown in Table 4 and Figure 19B, their membrane properties could clearly distinguish putative dopaminergic neurons in the SNc from neurons in the SNr. The SNc neurons were characterized by a low firing frequency, wide action potential width, and large sag potential in response to a hyperpolarizing current pulse (Table 4; Fig. 19B), consistent with earlier reports (Grace and Bunney 1983; Kita et al. 1986; Chuhma et al. 2011; Lammel et al. 2015). Moreover, by post-hoc TH immunohistochemical identification of the SNc, the recorded neurons (9/11 SNc neurons were well visualized with biocytin) were actually located in the TH-immunopositive SNc (Fig. 19A_2). TH immunoreactivity was directly detected in seven among nine recorded SNc neurons despite that the long recording duration usually prevented immunohistochemical detection (Fig. 19A_3). We investigated whether IPSC was elicited by photoactivation of ChR2-expressing PV-GP axon terminals. In 9 of 11 SNc neurons, IPSCs were evoked with latencies <2 ms from the beginning of LED exposure to the IPSC onset (Figs. 19C and 19D); from the remaining 2 neurons, IPSC was not detected. The amplitudes of evoked IPSCs varied widely among neurons (Fig. 19D), in line with

the biased distribution of PV-GP axon terminals in the SNc (Figs. 9, 11). Recorded SNc neurons were distributed from LM 2.4 to 1.4 mm, and no relationship was observed between the cell location along LM axis and IPSC strength. We further confirmed pharmacologically that the IPSCs were elicited by local activation of the PV-GP terminals. First, after applying a low-concentration of sodium channel blocker, tetrodotoxin (TTX, 1 μM) and potassium channel blocker, 4 amino-pyridine (4AP, 100 μM) to isolate monosynaptic responses (Shu et al. 2007; Petreanu et al. 2009), glutamate receptor antagonists (CNQX, 10 μM; AP5, 50 μM) were unable to affect the amplitudes of IPSCs (N = 3/3; Fig. 19C middle). Secondary, the IPSCs were completely blocked by an additional bath application of the $GABA_A$ receptor antagonist SR95531 (20 μM), as shown in the right column of Fig. 19C (N = 4/4). The IPSC amplitude decreased gradually during a series of 10 repeated photostimulations (5-ms pulses at 10 Hz; Figs. 19C, 19D, and1 9E), indicating short-term synaptic depression. Indeed, the 2nd and 10th IPSC amplitudes were 52.9% and 42.8% of the 1st amplitude, respectively, and these decreases were significant (Wilcoxon signed-rank test, $p = 0.008$ for both; Figs. 19D and 19E). This property was not related to the amplitude of the 1st IPSC and might be a common characteristic of PV-GP terminals in the SNc (Fig. 19E).

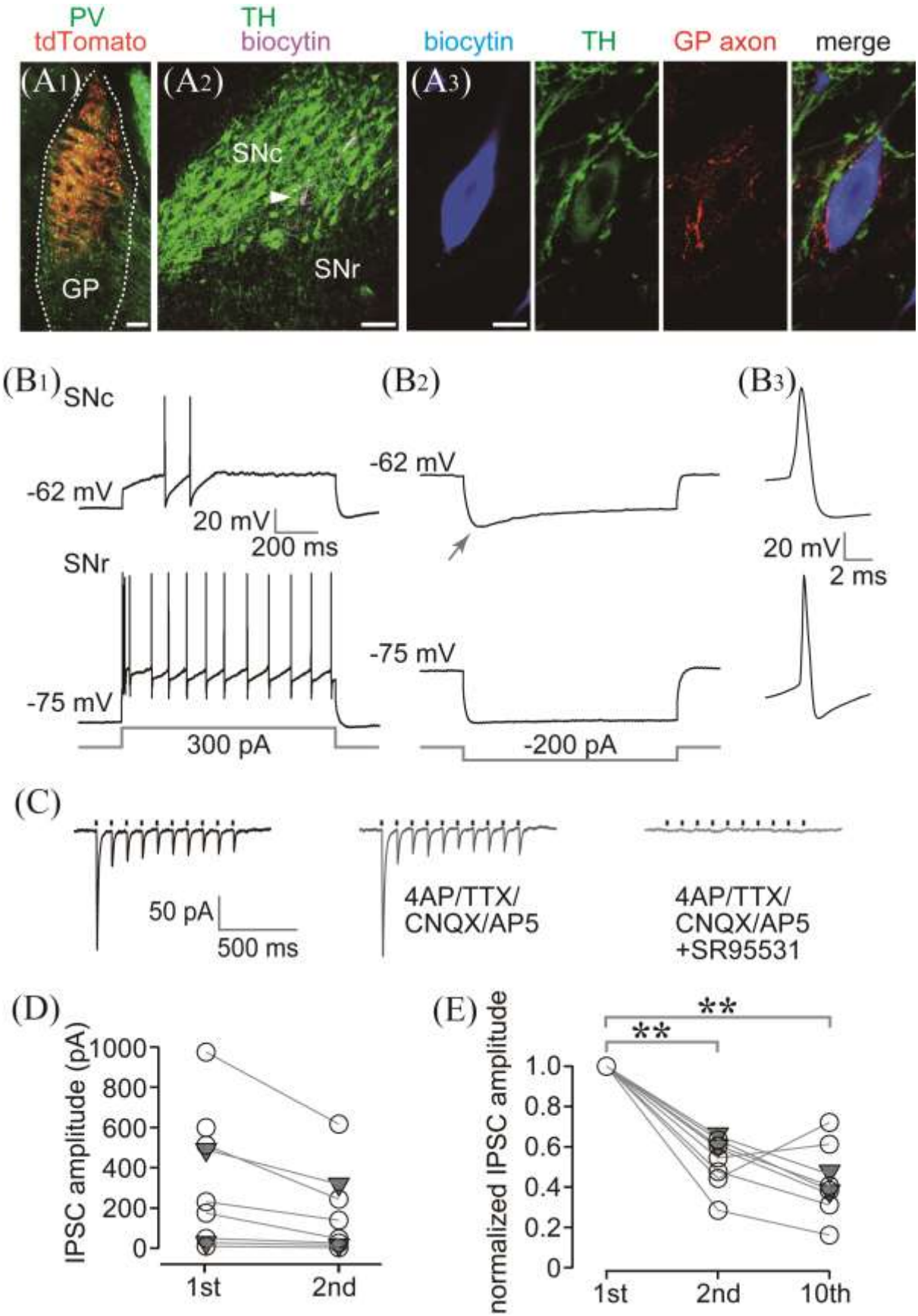

Fig. 19 Globus pallidus (GP) axon terminals of parvalbumin (PV) neurons elicited inhibitory postsynaptic currents (IPSCs) in substantia nigra pars compacta (SNc) dopaminergic neurons

(A) AAV injection into the GP for slice recording, and a representative recorded neuron in SNc.

(A1) AAV injection site in the GP. Scale bar, 200 μm. (A2) A recorded neuron (visualized with biocytin; arrowhead) in SNc. To clarify, the fluorescence of biocytin is shown in purple here. SNc was identified by TH immunoreaction (green). Scale bar, 100 μm. (A3) Confocal microscopic images for immunohistochemical identification of the recorded neuron shown in A2. The recorded neuron was visualized with biocytin (blue), which expressed TH (green). AAV labeled PV-GP axons (red) surrounded the neuron. A merged view is shown in the most right column. Scale bar, 10 μm. (B) Electrophysiological properties of SNc (upper) and SN reticulata (SNr; lower) neurons. (B1) Firing response induced by a depolarizing current pulse (300 pA for 1 s). Note the less frequent action potentials in the SNc neuron. (B2) Membrane voltage response by a hyperpolarizing current pulse (-200 pA for 1 s). Note the large sag potential in the SNc neuron (arrow). (B3) Magnified view of an action potential, which was wider in the SNc neuron vs. the SNr neuron. (C) Photo-activation of channel rhodopsin 2 (ChR2) in PV-GP axon terminals elicited IPSCs in a SNc neuron. Ten pulses of 5-ms blue light (470 nm) were applied at 10 Hz (short vertical line above the current traces) and reliably evoked IPSCs (left). Bath application of 4AP/TTX/CNQX/AP5 did not affect the IPSCs (middle), whereas SR95531 addition completely blocked IPSCs (right). The average traces of 10 repetitive sweeps are shown. (D) Amplitude of IPSCs in SNc neurons (N = 9 cells for 1st IPSC, N = 8 for 2nd IPSC). One neuron was stimulated by a single pulse. Gray triangle indicates a SNc neuron lacking immunoreactivity for TH after recording. (E) IPSCs exhibited short-term depression. The amplitudes of the 2nd and 10th IPSCs were normalized to that of the 1st IPSCs (N = 8 cells). The amplitude of the 1st IPSCs was significantly larger than those of the 2nd and 10th IPSC ($p = 0.008$ for both comparisons, Wilcoxon signed-rank test).

Table 4. Electrophysiological properties of SN neurons

	SNc	SNr
Number of neurons	11	3
Firing frequency (Hz)	2.4 ± 2.3	15, 88, 101
Resting membrane potential (mV)	-52.0 ± 6.0	-55.2, -71.5, -55.0
Input resistance (MΩ)	182.7 ± 69.0	211.2, 271.7, nd
Time constant (ms)	8.9 ± 3.8	7.5, 6.2, 8.3
Sag (mV)	10.2 ±6.7	1.3, 2.7, 5.2
Action potential width (ms)	2.15 ± 1.15	1.00, 0.96, 0.63
AHP amplitude (mV)	26.8 ± 7.6	22.3, 22.4, 23.1
IPSC amplitude (pA)	342 ± 325	no response

For SNc neurons, means ± standard deviations are shown. Values for each cell are presented for SNr neurons because of the small number of cells. nd, not determined. Firing frequency was determined as the maximum firing frequency evoked by a 1 s-depolarizing current pulse up to 1000 pA. No IPSC was recorded for SNr neurons because of the potentially small number of labeled terminals around the recorded cells (see text).

Chapter 4. Discussion

4. 1. Technical validation of the specificity of Cre expression in PV-Cre rats

In our PV-Cre rat model, the distribution of Cre in the CNS, including the cortex, hippocampus, Rt, and basal ganglia, was similar to that reported previously for PV mRNA (Kita 1994; Rajakumar et al. 1994; Hontanilla et al. 1997; Hoover and Marshall 2002; Mallet et al. 2012; Hernandez et al. 2015), and double immunostaining for Cre and PV expression in the GP showed that >80% of Cre neurons in our rats exhibited PV immunofluorescence (Fig. 4). Furthermore, Cre and PV expression were almost evenly matched in the lateral-medial axis of the GP (>80% each; bars in Fig. 3B). We note that PV-immunopositive neurons constituted approximately 38.8% of all GP neurons in the present study (Fig. 5), thus confirming previous reports in which approximately half of all neurons in the rat GP were found to express PV mRNA signals or immunoreactivity (Kita and Kitai 1994; Rajakumar et al. 1994; Hontanilla et al. 1997; Kita and Kita 2001; Hoover and Marshall 2002; Mallet et al. 2012; Abdi et al. 2015) and mice (Mastro et al. 2014; Dodson et al. 2015; Hernandez et al. 2015). However, 14% of the infected neurons were not PV-positive and approximately 20% PV neurons were not Cre positive. Although the distribution pattern of PV-GP axons in the present study was more similar to that of PV–GP axons, rather than Lhx6-GP axons, according to a previous report (Mastro et al. 2014), care should be taken to note that 20% of all Cre-immunopositive axons might have originated from non PV–GP neurons.

4. 2. Molecular architecture of GP neurons

Recent studies in Sprague–Dawley rats demonstrated that PV neurons comprised 59% of all GP neurons; in addition, 99% of PV neurons overlapped with Lhx6 expression (Abdi et al. 2015). This dichotomous cell classification is emphasized by the findings that $PV^{+}/Nkx2\text{-}1^{+}/Lhx6^{+}$ neurons comprised the major prototypic neurons and that $FoxP2^{+}$ neurons were arkypallidal neurons (Abdi et al. 2015). In the present study, which used PV-Cre and wild type Long Evans rats, as shown in Figure 5, PV neurons comprised approximately 39% of GP neurons, and 43% of PV neurons did not express Lhx6 in wild rats. Figure 8 also demonstrated AAV infected neurons rarely contained $Lhx6^{+}/PV^{-}$ neurons on GP sections. Given the lack of differences in data obtained from PV-Cre Long Evans rats and wild-type Long Evans rats (Table 3), this discrepancy might have originated in part from differences in the animal strains. Definition of GP area might also have contributed to this discrepancy. In a recent study, the ventral borders of GP in rostral and central sections were defined according to the medial edge of the anterior commissure and the bottom edge of the internal capsule, and the ventral border of GP in the caudal sections was defined according to the fornix (Abdi et al. 2015). In the present study, $Lhx6^{+}/ PV^{-}$ neurons were more abundant in GP ventral area than the dorsal area (Fig. 6). Therefore, it is possible that both the proportion of PV neurons in GP neurons and the co-expression rate of Lhx6 and PV would increase when the ventral area of GP is omitted. However, as observed in mice, the proportions of PV neurons range from 29% to 55%, and the frequencies of Lhx6 co-expression are highly variable (Nóbrega-Pereira et al. 2010; Mastro et al. 2014; Dodson et al. 2015; Hernandez et al. 2015).

Further data accumulation is necessary in both wild type and various lines of transgenic rodents. Similar to previous reports in both rats and mice, PV and FoxP2 co-expression was negligible in the present study (Figs. 5B and 5C; Flandin et al., 2010; Nóbrega-Pereira et al., 2010; Abdi et al., 2015; Dodson et al., 2015; Hernandez et al., 2015). The present results also suggested that PV neurons could be further divided into PV+/Lhx6+ and PV+/Lhx6– and less than half of Lhx6+ neurons expressed PV in our experiment (but see Abdi et al. 2015). Therefore using the PV-Cre rat line, we could select only PV-GP neuronal population among prototypic neurons.

4. 3. Projection of pallidonigral neurons

4. 3. 1. Pallidonigral projections preferentially innervate the ventral tier of SNcd

Regarding the topographical organization of pallidonigral projections in the rat, previous anterograde tracing studies have demonstrated that the lateral part of GP profusely projects to the central core of the rostral three-quarters of SNr (Smith and Bolam 1989), whereas the ventral pallidum preferentially projects to the medial part of SNc, rather than the medial part of SNr (Groenewegen et al. 1993). Because striatal axons might take up the tracer injected into GP, it could be difficult to distinguish pallidonigral and striatal axons using classical anterograde tracing methods. Because PV neurons in the striatum and GP are interneurons and projection neurons, respectively, studies of PV-Cre transgenic mice allow the specific analysis of PV-GP projections versus projections from striatal projection neurons (Mastro et al. 2014; Hernandez et al. 2015). Normalized axon fluorescence intensity allowed the finding that in the mouse SNc, GP axons arose

from mostly Lhx6-expressing neurons, with few arising from PV-expressing neurons, even though both Lhx6 and PV axons were concentrated in the dorsal SN, particularly along the border region between the SNc and SNr (Fig. 5C in Mastro et al., 2014). However, as dopamine neurons possess dendrites that extend into the SNr in these areas, investigations to determine whether dopamine or GABA neurons comprise the postsynaptic elements innervated by GP axons must be conducted carefully. Interestingly, these dense terminations were scattered throughout the SN, especially in the ventral part of SNcd (Figs. 10 and 11), where CB^{+}/TH^{+} neurons rarely existed. It could be a characteristic nature of PV-GP projections, although alternatively it might come from topographic projection patterns and PV-GP neurons outside of our injection area, ex. the ventral part of the GP, might innervate the dorsal portion of SNc. We, however, think it is not likely the case because as shown in Figs. 10-12, increasing AAV infection area in the GP mainly resulted in increment of number of terminals, and not in topographical rearrangement.

4. 3. 2. Pallidonigral projections formed basket-like somatic apposition

In the present study, we generated a novel PV-Cre rat model and carefully analyzed PV-GP axons in the SN morphologically and electrophysiologically (Figs. 10-12 and 17-19). Similar to the previous report (Mastro et al. 2014), PV-GP neurons formed dense axon varicosities in the border region between the SNcd and SNr yet arborized loosely as long collaterals featuring basket-like appositions with PV somata and dendrites of PV positive cells in SNr (Figs. 17 and 18). Together with data from triple immunostaining of TH, PV, and gephyrin (an inhibitory postsynaptic marker), we revealed that axons from PV–GP neurons, which co-localized with gephyrin, formed somatic

appositions on TH and PV neurons in SN. Electrophysiological experiments confirmed PV-GP axons provided functional inhibitory synapses on SNc (Fig. 19). The EP/SNr receives a large amount of GP input at the level of the perikaryon, whereas terminals derived from the striatum and STN are relatively evenly distributed throughout neuron domains (for review, Smith et al., 1998). However, it is not clear which type of GP neurons form these axo-somatic synapses. In the present study, we revealed that the PV-GP axonal boutons were concentrated around the cell bodies of PV^+, CCK^+ and CR^+ neurons as well as with TH^+ dopaminergic neurons (Figs. 13-16). This cell domain selectivity looks similar to PV neurons in the neocortex and the neostriatum, which are frequently innervated cell body domains of target neurons (for review, Kubota et al., 2016). Because the somatic synapse is large in size and the synaptic release probability correlates with synaptic size (Holderith et al. 2012), PV–GP terminals on SN would have a high probability of release. This idea is supported by the observation of paired pulse depression in the synapse (Fig. 19D, E). Notably PV-GP axons exhibited a clear preference for dopamine neurons in the ventral part of SNcd (Figs.10-12).

4.3.3. PV-GP neurons inhibit to dopaminergic neurons in SNc

Whole-cell patch clamp with ChR2-photostimulation revealed that PV-GP axons strongly inhibited dopaminergic neurons via $GABA_A$ receptors, as shown in vivo unit recording (Paladini et al. 1999). Therefore, both morphologic and electrophysiological methods revealed that multiple somatic synapses of presynaptic PV-GP terminals were concentrated on single postsynaptic dopaminergic neurons in the SNc. PV-GP to SNc synapses were strongly depressed even at stimulation with 10

Hz (Figs. 19 C, D, and E). Because PV-GP neurons were found to fire spontaneously at an average of 20–30 Hz in vivo (Mallet et al. 2012; Abdi et al. 2015), PV-GP-SNc synapses might become depressed in response to repetitive firings. The synapse may be fully activated on the first spike while recovering from inhibition by striatal indirect medium spiny neurons (MSNs).

4. 3. 4. Roll of pallidonigral projection in the BG network model

PV-GP projections also innervated a SNr side at the border (beneath the SNc), which corresponds with the "insular-peripheral orbital (caudal)" and "medial orbital and prelim ventral (rostral)" areas (Deniau et al. 2007). From a cell-specific retrograde tracing study, Watabe-Uchida et al. reported that GP projected predominantly to SNc dopamine neurons, whereas the ventral pallidum and sublenticular extended amygdala projected predominantly to dopamine neurons in the ventral tegmental area (Watabe-Uchida et al. 2012). Further reports indicate that separate groups of dopamine neurons with distinct projection targets were largely separated topographically in both mice and primates (Kim et al. 2014; Kim and Hikosaka 2015; Menegas et al. 2015). For example, GP projected to a subgroup of dopamine neurons, which in turn projected to the tail of the striatum (Menegas et al., 2015). In the present study, dense PV-GP terminations observed around dopamine neurons might reflect a unique input/output organization in the basal ganglia. On the other hand, striatum-SNc inhibition originates from direct pathway MSNs that express the D1 receptor, whereas the D2, D3, D4, and D5 receptors are expressed in the perikarya and dendrites of GP neurons (Mrzljak et al. 1996; Khan et al. 1998; Khan et al. 2000). Therefore, these pathways might exert different modes of dopaminergic modulation; and their timing, plasticity, and functional

significance will be investigated further in future.

Chapter 5. References

1. Abdi A, Mallet N, Mohamed FY, et al (2015) Prototypic and Arkypallidal Neurons in the Dopamine-Intact External Globus Pallidus. J Neurosci 35:6667–6688. doi: 10.1523/JNEUROSCI.4662-14.2015
2. Atasoy D, Aponte Y, Su HH, Sternson SM (2008) A FLEX switch targets Channelrhodopsin-2 to multiple cell types for imaging and long-range circuit mapping. J Neurosci 28:7025– 7030. doi: 10.1523/JNEUROSCI. 1954-08.2008
3. Bergman H, Feingold A, Nini A, et al (1998) Physiological aspects of information processing in the basal ganglia of normal and parkinsonian primates. Trends Neurosci. 21:32–38.
4. Bevan MD, Booth P a, Eaton S a, Bolam JP (1998) Selective innervation of neostriatal interneurons by a subclass of neuron in the globus pallidus of the rat. J Neurosci 18:9438–52.
5. Bevan MD, Magill PJ, Terman D, et al (2002) Move to the rhythm: Oscillations in the subthalamic nucleus-external globus pallidus network. Trends Neurosci. 25:525–531.
6. Bevan MD, Smith AD, Bolam JP (1996) The substantia nigra as a site of synaptic integration of functionally diverse information arising from the ventral pallidum and the globus pallidus in the rat. Neuroscience 75:5–12. doi: 10.1016/0306-4522(96)00377-6
7. Bolam JP, Smith Y (1990) The GABA and substance P input to dopaminergic neurones in the substantia nigra of the rat. Brain Res 529:57–78. doi: 10.1016/0006-8993(90)90811-O
8. Carter DA, Fibiger HC (1978) The projections of the entopeduncular nucleus and globus pallidus in rat as demonstrated by autoradiography and horseradish peroxidase histochemistry. J Comp Neurol 177:113–23. doi: 10.1002/cne.901770108
9. Chuhma N, Tanaka KF, Hen R, Rayport S (2011) Functional connectome of the striatal medium spiny neuron. J Neurosci 31:1183–1192. doi: 10.1523/JNEUROSCI.3833-10.2011
10. DeFelipe J (1993) A study of NADPH diaphorase-positive axonal plexuses in the human temporal cortex. Brain Res 615:342–346. doi: 10.1016/0006-8993(93)90047-Q

11. DeLong MR, Crutcher MD, Georgopoulos AP (1985) Primate globus pallidus and subthalamic nucleus: functional organization. J Neurophysiol 53:530–543.
12. Deniau JM, Mailly P, Maurice N, Charpier S (2007) The pars reticulata of the substantia nigra: a window to basal ganglia output. Prog. Brain Res. 160:151–172.
13. DeVito J, Anderson M (1982) An autoradiographic study of efferent connections of the globus pallidus in Macaca mulatta. Exp brain Res Exp Hirnforsch e 46:107–17.
14. Dodson PD, Larvin JT, Duffell JM, et al (2015) Distinct developmental origins manifest in the specialized encoding of movement by adult neurons of the external globus pallidus. Neuron 86:501–513. doi: 10.1016/j.neuron.2015.03.007
15. Flandin P, Kimura S, Rubenstein JL (2010) The progenitor zone of the ventral medial ganglionic eminence requires Nkx2-1 to generate most of the globus pallidus but few neocortical interneurons. J Neurosci 30:2812–2823. doi: 10.1523/JNEUROSCI.4228-09.2010
16. Gerfen CR, Staines W a, Arbuthnott GW, Fibiger HC (1982) Crossed connections of the substantia nigra in the rat. J Comp Neurol 207:283–303. doi: 10.1002/cne.902070308
17. Gittis AH, Berke JD, Bevan MD, et al (2014) New Roles for the External Globus Pallidus in Basal Ganglia Circuits and Behavior. J Neurosci 34:15178–15183. doi: 10.1523/JNEUROSCI.3252-14.2014
18. Grace AA, Bunney BS (1983) Intracellular and extracellular electrophysiology of nigral dopaminergic neurons-1. Identification and characterization. Neuroscience. 10:301-15. doi:10.1016/0306-4522(83)90135-5
19. Groenewegen HJ, Berendse HW, Haber SN (1993) Organization of the output of the ventral striatopallidal system in the rat: Ventral pallidal efferents. Neuroscience 57:113–142. doi: 10.1016/0306-4522(93)90115-V
20. Haber SN, Lynd-Balta E, Mitchell SJ (1993) The organization of the descending ventral pallidal projections in the monkey. J Comp Neurol 329:111–128. doi: 10.1002/cne.903290108
21. Haber SN, Watson SJ (1985) The comparative distribution of enkephalin, dynorphin and

substance P in the human globus pallidus and basal forebrain. Neuroscience 14:1011–1024. doi: 10.1016/0306-4522(85)90272-6

22. Hernandez VM, Hegeman DJ, Cui Q, et al (2015) Parvalbumin+ Neurons and Npas1+ Neurons Are Distinct Neuron Classes in the Mouse External Globus Pallidus. J Neurosci 35:11830–11847. doi: 10.1523/JNEUROSCI.4672-14.2015
23. Holderith N, Lorincz A, Katona G, et al (2012) Release probability of hippocampal glutamatergic terminals scales with the size of the active zone. Nat Neurosci 15:988–97. doi: 10.1038/nn.3137
24. Hontanilla B, Parent A, Giménez-Amaya JM (1997) Parvalbumin and calbindin D-28k in the entopeduncular nucleus, subthalamic nucleus, and substantia nigra of the rat as revealed by double- immunohistochemical methods. Synapse 25:359–367. doi: 10.1002/(SICI)1098-2396(199704)25:4<359::AID-SYN7>3.0.CO;2-9
25. Hoover BR, Marshall JF (2002) Further characterization of preproenkephalin mRNA-containing cells in the rodent globus pallidus. Neuroscience 111:111–125. doi: 10.1016/S0306-4522(01)00565-6
26. Jaeger D, Gilman S, Wayne Aldridge J (1995) Neuronal activity in the striatum and pallidum of primates related to the execution of externally cued reaching movements. Brain Res 694:111–127. doi: 10.1016/0006-8993(95)00780-T
27. Khan ZU, Gutiérrez A, Martín R, Peñafiel A, Rivera A, de la Calle A (2000) Dopamine D5 receptors of rat and human brain. Neuroscience 100:689–699. doi: 10.1016/S0306-4522(00)00274-8
28. Khan ZU, Gutiérrez A, Martín R, Peñafiel A, Rivera A, de la Calle A (1998) Differential regional and cellular distribution of dopamine D2-like receptors: An immunocytochemical study of subtype-specific antibodies in rat and human brain. J Comp Neurol 402:353–371. doi: 10.1002/(SICI)1096-9861(19981221)402:3<353::AID-CNE5>3.0.CO;2-4
29. Kim HF, Ghazizadeh A, Hikosaka O (2014) Separate groups of dopamine neurons innervate

caudate head and tail encoding flexible and stable value memories. Front Neuroanat 8:120. doi: 10.3389/fnana.2014.00120

30. Kim HF, Hikosaka O (2015) Parallel basal ganglia circuits for voluntary and automatic behaviour to reach rewards. Brain 138:1776–1800. doi: 10.1093/brain/awv134
31. Kim R, Nakano K, Jayaraman A, Carpenter MB (1976) Projections of the globus pallidus and adjacent structures: an autoradiographic study in the monkey. JComp Neurol 169:263–290. doi: 10.1002/cne.901690302
32. Kincaid AE, Penney JB, Young AB, Newman SW (1991) Evidence for a projection from the globus pallidus to the entopeduncular nucleus in the rat. Neurosci Lett 128:121–125. doi: 10.1016/0304-3940(91)90774-N
33. Kita H (1994) Parvalbumin-immunopositive neurons in rat globus pallidus: a light and electron microscopic study. Brain Res 657:31–41. doi: 10.1016/0006-8993(94)90950-4
34. Kita H (2007) Globus pallidus external segment. Prog. Brain Res. 160:111–133.
35. Kita H, Kitai ST (1994) The morphology of globus pallidus projection neurons in the rat: an intracellular staining study. Brain Res 636:308–319. doi: 10.1016/0006-8993(94)91030-8
36. Kita H, Kita T (2001) Number, origins, and chemical types of rat pallidostriatal projection neurons. J Comp Neurol 437:438–448. doi: 10.1002/cne.1294
37. Kita H, Kitai ST (1991) Intracellular study of rat globus pallidus neurons: membrane properties and responses to neostriatal, subthalamic and nigral stimulation. Brain Res 564:296–305. doi: 10.1016/0006-8993(91)91466-E
38. Kita T, Kita H, Kitai ST (1986) Electrical membrane properties of rat substantia nigra compacta neurons in an in vitro slice preparation. Brain Res 372:21–30. doi: 10.1016/0006-8993(86)91454-X
39. Klausberger T, Somogyi P (2008) Neuronal diversity and temporal dynamics: the unity of hippocampal circuit operations. Science 321:53–7. doi: 10.1126/science.1149381
40. Kubota Y, Karube F, Nomura M, Kawaguchi Y (2016) The Diversity of Cortical Inhibitory

Synapses. Front Neural Circuits 10:1–15. doi: 10.3389/fncir.2016.00027

41. Lammel S, Steinberg EE, Földy C, et al (2015) Diversity of transgenic mouse models for selective targeting of midbrain dopamine neurons. Neuron 85:429–438. doi:10.1016/j.neuron.2014.12.036
42. Mallet N, Micklem BR, Henny P, et al (2012) Dichotomous Organization of the External Globus Pallidus. Neuron 74:1075–1086. doi: 10.1016/j.neuron.2012.04.027
43. Mastro KJ, Bouchard RS, Holt H a K, Gittis AH (2014) Transgenic mouse lines subdivide external segment of the globus pallidus (GPe) neurons and reveal distinct GPe output pathways. J Neurosci 34:2087–2099. doi: 10.1523/JNEUROSCI.4646-13.2014
44. McBride RL, Larsen KD (1980) Projections of the feline globus pallidus. Brain Res 189:3–14. doi: 10.1016/0006-8993(80)90003-7
45. Menegas W, Bergan JF, Ogawa SK, et al (2015) Dopamine neurons projecting to the posterior striatum form an anatomically distinct subclass. eLife 4:1–30. doi: 10.7554/eLife.10032
46. Miyamoto Y, Fukuda T (2015) Immunohistochemical study on the neuronal diversity and three-dimensional organization of the mouse entopeduncular nucleus. Neurosci Res 94:37–49. doi: 10.1016/j.neures.2015.02.006
47. Mounir S, Parent A (2002) The expression of neurokinin-1 receptor at striatal and pallidal levels in normal human brain. Neurosci Res 44:71–81. doi: 10.1016/S0168-0102(02)00087-1
48. Mrzljak L, Bergson C, Pappy M, et al (1996) Localization of dopamine D4 receptors in GABAergic neurons of the primate brain. Nature 381:245–8.
49. Nambu A, Llinas R (1994) Electrophysiology of globus pallidus neurons in vitro. JNeurophysiol 72:1127–1139.
50. Nambu A, Llinás R (1997) Morphology of globus pallidus neurons: Its correlation with electrophysiology in guinea pig brain slices. J Comp Neurol 377:85–94. doi: 10.1002/(SICI)1096-9861(19970106)377:1<85::AID-CNE8>3.0.CO;2-F
51. Nauta HJW (1979) Projections of the pallidal complex: An autoradiographic study in the cat.

Neuroscience 4:1853–1873. doi: 10.1016/0306-4522(79)90060-5

52. Nóbrega-Pereira S, Gelman D, Bartolini G, et al (2010) Origin and molecular specification of globus pallidus neurons. J Neurosci 30:2824–2834. doi: 10.1523/JNEUROSCI.4023-19 09.2010

53. Paladini CA, Celada P, Tepper JM (1999) Striatal, pallidal, and pars reticulata evoked inhibition of nigrostriatal dopaminergic neurons is mediated by GABA(A), receptors in vivo. Neuroscience 89:799–812. doi: 10.1016/S0306-4522(98)00355-8

54. Parent A, Hazrati LN (1995a) Functional anatomy of the basal ganglia. I. The cortico-basal ganglia-thalamo-cortical loop. Brain Res. Rev. 20:91–127.

55. Parent A, Hazrati LN (1995b) Functional anatomy of the basal ganglia. II. The place of subthalamic nucleus and external pallidium in basal ganglia circuitry. Brain Res. Rev. 20:128–154.

56. Paxinos G, Watson C (2007) The rat brain in stereotaxic coordinates. 6th Ed. Academic Press, San Diego.

57. Paxinos G, Watson C, Carrive P, Kirkcaldie M, Ashwell KWS (2009) Chemoarchitectonic atlas of the rat brain. Second edition. Academic Press, San Diego.

58. Petreanu L, Mao T, Sternson SM, Svoboda K (2009) The subcellular organization of neocortical excitatory connections. Nature 457:1142–5. doi: 10.1038/nature07709

59. Rajakumar N, Rushlow W, Naus CCG, et al (1994) Neurochemical compartmentalization of the globus pallidus in the rat: An immunocytochemical study of calcium-binding proteins. J Comp Neurol 346:337–348. doi: 10.1002/cne.903460303

60. Robledo P, Ferger J (1990) Excitatory influence of rat subthalamic nucleus to substantia nigra pars reticulata and the pallidal complex: electrophysiological data. Brain Res 518:47–54. doi: 10.1016/0006-8993(90)90952-8

61. Sadek AR, Magill PJ, Bolam JP (2007) A single-cell analysis of intrinsic connectivity in the rat globus pallidus. J Neurosci 27:6352–62. doi: 10.1523/JNEUROSCI.0953-07.2007

62. Shu Y, Yu Y, Yang J, McCormick D a (2007) Selective control of cortical axonal spikes by a slowly inactivating K+ current. Proc Natl Acad Sci U S A 104:11453–11458. doi: 10.1073/pnas.0702041104

63. Smith AD, Bolam JP (1990a) The neural network of the basal ganglia as revealed by the study of synaptic connections of identified neurones. Trends Neurosci 13:259–265. doi: 10.1016/0166-2236(90)90106-K

64. Smith Y, Bevan MD, Shink E, Bolam JP (1998) Microcircuitry of the direct and indirect pathways of the basal ganglia. Neuroscience 86:353–387. doi: 10.1016/S0306-4522(98)00004-9

65. Smith Y, Bolam JP (1989) Neurons of the substantia nigra reticulata receive a dense GABAcontaining input from the globus pallidus in the rat. Brain Res 493:160–167. doi: 10.1016/0006-8993(89)91011-1

66. Smith Y, Bolam JP (1990b) The output neurones and the dopaminergic neurones of the substantia nigra receive a GABA-containing input from the globus pallidus in the rat. J Comp Neurol 296:47–64. doi: 10.1002/cne.902960105

67. Stephenson-Jones M, Samuelsson E, Ericsson J, et al (2011) Evolutionary conservation of the basal ganglia as a common vertebrate mechanism for action selection. Curr Biol 21:1081–1091. doi: 10.1016/j.cub.2011.05.001

68. Tanahira C, Higo S, Watanabe K, et al (2009) Parvalbumin neurons in the forebrain as revealed by parvalbumin-Cre transgenic mice. Neurosci Res 63:213–223. doi: 10.1016/j.neures.2008.12.007

69. Tepper JM, Lee CR (2007) GABAergic control of substantia nigra dopaminergic neurons. Prog. Brain Res. 160:189–208.

70. Tepper JM, Martin LP, Anderson DE (1995) GABAA re-cep-tor-me-di-ated in-hi-bi-tion of rat sub-stan-tia nigra dopamin-er-gic neu-rons by pars retic-u-lata pro-jec-tion neu-rons. J Neurosci 15:3092–3103.

71. Watabe-Uchida M, Zhu L, Ogawa SK, et al (2012) Whole-Brain Mapping of Direct Inputs to Midbrain Dopamine Neurons. Neuron 74:858–873. doi: 10.1016/j.neuron.2012.03.017

72. Wheeler DW, White CM, Rees CL, et al (2015) Hippocampome.org: A knowledge base of neuron types in the rodent hippocampus. eLife. doi: 10.7554/eLife.09960

73. Wichmann T, Bergman H, DeLong MR (1994) The primate subthalamic nucleus. III. Changes in motor behavior and neuronal activity in the internal pallidum induced by subthalamic inactivation in the MPTP model of parkinsonism. J Neurophysiol 72:521–530.